Scanning Electron Microscopy

Volume 1982
Number 1 *1982*

Article 6

1982

Interaction of Electron Beam with the Target in Scanning Electron Microscope

Koichi Kanaya
Kogakuin University

Susumu Ono
Elicnix Co. Ltd.

Electron Beam Interactions With Solids (Pp. 69-98)
SEM, Inc., AMF O'Hare (Chicago), IL 60666, U.S.A.

INTERACTION OF ELECTRON BEAM WITH THE TARGET IN SCANNING ELECTRON MICROSCOPE

Koichi Kanaya and Susumu Ono*

Kogakuin University, 1-24-2, Nishishinjuku, Shinjuku-ku, Tokyo, Japan
* Elionix Co. Ltd., Nishihachioji, Hachioji, Tokyo, Japan

Abstract

Based on the fundamental potential function of the power and exponential forms, a diffusion model of electron beams penetrating in a target has been proposed to take place throughout a hemisphere with a centre located at the most probable energy dissipation depth, related to the diffusion depth and the maximum energy dissipation depth, which is found to agree well with the empirical data of back-scattering coefficient as a function of the incident energy.

Based on the energy retardation power formula concerning the penetration and the energy loss of an electron probe into solid targets, the secondary electron emission yield has been derived as functions of three parameters such as atomic number, first ionization (or plasmon loss for an insulator) and back-scattering coefficient.

Accordingly, the energy-and angular-dependence of secondary electron emissions and the subsequent temperature-rise of the specimens are quantitatively discussed for various target materials in SEM.

KEY WORDS: diffusion model, backscattered electrons, secondary electron emission, energy loss, range, temperature-rise, resolving power, back-scattering coefficient, range-energy relation, electron transmission, diffusion depth, absorption of electrons, energy dissipation, escape depth, secondary electron yield.

Address correspondence to:

Koichi Kanaya
Kogakuin University
1-24-2, Nishishinjuku,
Shinjuku-ku, Tokyo, Japan

Phone No. 03-342-1211

I The Energy Dependence of a Diffusion Model for an Electron Probe into Solid Targets

1. Introduction

Since the publication of Lenard(1895), an explanation of the phenomena connected with electron penetration into solid materials has required quantitative information about the attenuation of the electrons, especially with the increasing use of scanning electron microscopy and electron probe microanalysis.

The first theoretical expression for the stopping power of electrons in solids was developed by Bethe (1933) using classical quantum theory. The work by Pines and Bohm (1952) and Ritchie(1973) based on plasmon excitation in solids, and by Ferrell (1956) and Marton et al (1954) using electron transitions in solids provided results similar to Bethe's formula. Accordingly, many authors used this stopping power formula for energy transfer. Theories based on simple collision models were developed by Everhart (1960), Archard (1961),Cosslett and Thomas (1964a,b),Nakhotkin et al(1962,63,65)and Everhart and Hoff (1971) using energy integrations as well as scattering cross-sections. More exact results were obtained in the previous work of Kanaya and Okayama (1972) and Kanaya and Kawakatsu (1972) who showed how the Lindhard power potential depended on the incident energy. Similar models by Vyatskin and Trunev (1967) and Dupouy et al(1964, 1965) were presented using the experimental work of Fitting (1974).

However, none of these models covers the whole wide energy range so it is not always easy to determine the scattering characteristics. An attempt to provide a more complete analysis has been shown by Kanaya and Ono (1978).

When a stream of electrons penetrates into a solid target, electrons may be scattered either elastically or inelastically. 'Electronic stopping' is due to an inelastic collision with atomic electrons in which the incident electron excites or ejects atomic electrons with loss of energy.

'Nuclear stopping' arises from nearly elastic collisions with atomic nuclei, with transfer of both energy and momentum. Thus electrons travel straight into the diffusion depth in the target, suffering energy loss due to the electronic collisions (small-angle scattering), and are also deflected by the nuclear collisions (large-angle scattering).

The plasmon excitation also affects the energy loss of electrons in the solid. Even though the cross-section of plasmon excitation is greater, the energy loss seems to be generally small compared with the energy dissipation due to the electronic collision in the thick targets. The probability of the energy spectrum of the plasmon $p_k(t)$ that k quanta are lost in a foil thickness t is given by the Poisson distribution by Blackstock et al (1955), i.e.

$$p_k(t)=\frac{1}{k!}\left(\frac{t}{\Lambda}\right)^k \exp\left(-\frac{t}{\Lambda}\right)$$

where Λ is the mean free path for loss of a quantum of energy $\hbar\omega_p$ in the thickness t. The plasmon loss (15-30 eV) is smaller than the average ionisation loss depending on Z (100-200 eV, Rauth and Simpson 1964), so the plasmon effects can be neglected for a solid target except insulators.

It is clearly desirable to have as accurate an analytical approximation to the atomic potential as possible. Therefore, a potential function V(r) as a function of the screened atomic radius a, consisting of the power and exponential forms is used:

$$V(r)=(Ze^2/a)(r/a)^{[(1/n)-2]}\exp(-r/a) \qquad (1)$$

where $a=0{\cdot}77\,a_H Z^{-1/6}$ (Å), e is the electronic charge, Z the atomic number, a_H the first Bohr radius of hydrogen, and n indicates the degree of screening (n goes from 1 to ∞ as the accelerating voltage decreases).

For n=1, (1) corresponds to the Wentzel atomic scattering theory and Bethe's energy loss law is satisfied. The atomic number dependence of a assumed above is very close to the results of quantitative electron microscopy achieved by Zeitler and Bahr(1959) rather than the result of X-ray absorption used by Lenz (1954): i.e. $a=a_H Z^{-1/3}$ (Å).

The value of n as a function of the incident energy E and the value of a can both be empirically determined by comparing the quantitative theoretical and experimental results, such as mass-range (Kanaya and Kawakatsu 1972), energy loss and complex scattering amplitude (Kanaya and Ono 1976). The value of n is given as a function of the incident energy E for various target materials where the parameter is numerically formulated as

$$n=1+2\exp(-\xi+2\times10^{-\xi}) \qquad (2)$$

with $\xi=\lg(\epsilon_l/2)$ and $\epsilon_l=a/b$, where ϵ_l is defined as the reduced energy (dimensionless) and b is the so-called 'collision diameter' (given by $b=2e^2/E$ $=4a_H E_R/E$, E_R being the Rydberg energy).

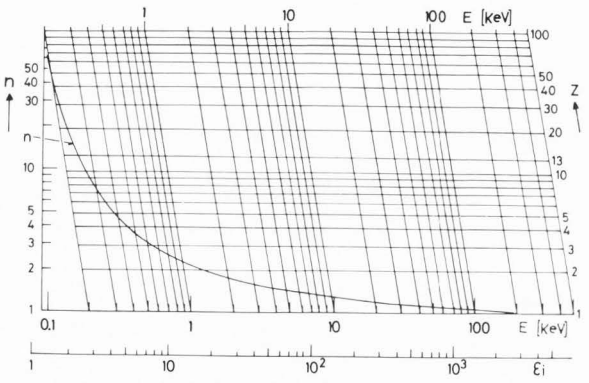

Figure 1. The parameter n as functions of the incident energy E and the reduced energy ε_i for the parameter of atomic number Z.

Figure 1 shows the value of n *versus* the incident energy E and the reduced energy ε_i for the parameter of atomic number Z.

The inelastic scattering amplitude can also be calculated using the interaction potential based on the same scheme:

$$V_{os}(r)=(e^2/a)(r/a)^{[(1/n)-2]}\exp(-r/a)$$

where 'os' indicates the transition from the state 's' by the impact.

Accordingly, the resulting elastic and inelastic scattering cross-sections can be integrated over the scattering angles.

Following the previous procedure used by the author in 1972, the semi-empirical expressions for the fractions of transmission η_T, backscattering η_B and absorbed energy E_A can be obtained as functions of the reduced depth $y=x/R$ and the parameter γ (as described in section 4 in detail) which are used for different target materials and over a wide energy range, as parameters Z and n, respectively. Furthermore, after comparing the results obtained by the present theory with the diffusion model, the most important characteristics of a diffusion model such as y_D, y_E, y_C, the back-scattering coefficient r, the absorbed energy E_A and the back-scattering energy E_B can be derived as a function of γ.

2. Elastic and inelastic scattering cross-section

By substituting the analytical fits to the potential (1) into a first Born approximation, the result for elastic cross-section inside the limiting angle α due to nuclear collision as well as electronic collision is as follows (Kanaya and Ono 1976):

$$\sigma_e=\frac{4}{n}\pi Z^2\Gamma^2\left(\frac{1}{n}\right)a^2(a_H/a)^{2/n}(E_R/E)^{1+1/n}\times[(1+2\epsilon E)^2/(1+\epsilon E)^{1+1/n}]$$
$$\times\left(1+\frac{1}{Z}\right) \qquad (3)$$

where ϵ is the relativistic correction factor given the well-known relationship $\epsilon = e/(2m_0c^2) = 0{\cdot}978 \times 10^{-6}\ \mathrm{eV}^{-1}$, E the incident energy of electrons [eV], and $\Gamma(1/n)$ is the Gamma function.

The final factor in the above eq. (1+1/Z), indicates the effect of the elastic scattering of incident electrons with free electrons; this cannot be disregarded for light elements. When we consider the electron penetration in the target, electrons suffering deflections of more than 90° do not travel into the subsequent layers of the target and the cross-section is given by integration from $\theta = 0°$ to 90° as a first approximation. As was pointed out by Archard (1961), many electrons are deflected between 0° and 90°, and some of them are lost by a multiple collision effect. Consider an electron initially deflected at 45°: at most it can suffer a second deflection of 45° in the opposite sense to get back into its original direction, but it might equally be deflected by 45° in the same direction, thereby acquiring a total 90° and becoming lost to subsequent layers. Thus a second approximation for the cross-section has been derived by adding half the integration from 90°to $3\pi/4$. But the correction may not be enough, since the triple and more collisions must exist in fact, as shown in Figure 2. A better approximation may be derived using the equation

$$\Omega = \frac{1}{3}\left(\int_0^{\pi/2} d\Omega + \frac{1}{2!}\int_{\pi/2}^{3\pi/4} d\Omega + \frac{1}{3!}\int_{\pi/2}^{5\pi/8} d\Omega\right) \qquad (4)$$

where $d\Omega = \sin\theta\, d\theta/(1+\cos\theta)^{1+1/n}$. Then the total scattering cross-section for the angular deflection due to multiple elastic collisions can be expressed by

$$\sigma = \sigma_e \Omega\ . \qquad (5)$$

The differential cross-section for energy loss due to electronic collision is

$$T_m \frac{d\sigma_i}{dT} = \frac{\lambda_n^2\, \Gamma^2(1/n)\, 4\, Z\pi (a/a_H)^2 \sin^2[(1/n)(\pi/2-\phi)]}{k^2\theta^2[1+(\theta/\theta_0)^2]^{1/n}} \qquad (6)$$

where T is the energy transfer with the maximum value T_m, $T/T_m = 4\sin^2(\theta/2) = \theta^2$, $\tan^{-1}\phi = a(k_0^2 + k_s^2 - 2k_0k_s\cdot\cos\theta)^{1/2}$, $\theta_0 = \lambda/(2\pi a)$, θ being the scattering angle in the centre-of-gravity system, λ the wavelength of the electron and λ_n the scaling correction factor for low-electron energy.

Substituting $d\sigma_i/dT$ from (6), the average energy loss dE/dx is calculated using $dE/dx = N\int T(d\sigma_i/dT)\,dT$. This gives

$$\frac{dE}{dx} = \left[NZ\pi 4\,\Gamma^2\left(\frac{1}{n}\right)\lambda_n^2 a^{2-2/n} a_H^{2/n} E_R^{1+1/n} E^{-1/n}\left(\frac{n}{n-1}\right)\frac{(1+2\epsilon E)^2}{(1+\epsilon E)^{1+1/n}}\right] \times\left[1-\left(\frac{E_I(1+2\epsilon E)}{4E(1+\epsilon E)}\right)^{1-1/n}\right]. \qquad (7)$$

where N is the number of atoms per unit volume in the target; $N = N_a\rho/A$, N_a is the Avogadro number, ρ the atomic density, A the atomic weight, E_I the suitably averaged excitation energy (for experimental example $E_I = 100\text{-}200\mathrm{eV} = 20E_R$, Rauth and Simpson 1964).

Equations (3) and (7) are the fundamental equations of elastic and inelastic scattering theory.

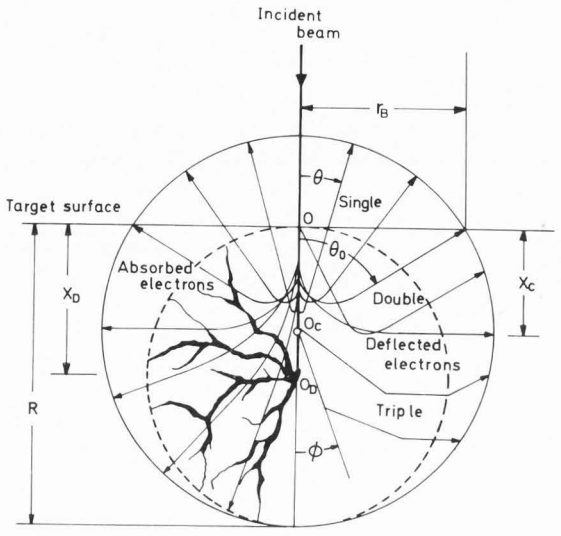

Figure 2. Diffusion model of electron beam penetration in a target: R is the maximum range; x_D the diffusion depth; x_C the most probable energy dissipation depth; r_B the back-scattering range; $\tan\theta_0 = r_B/x_C$.

3. The range-energy relationship

The maximum range can be derived from the energy-loss equation:

$$R = \int_0^{E_0} \frac{dE}{(dE/dx)} = \frac{(n-1)E_0^{1+1/n}(1+\epsilon E_0)^{1+1/n}}{NZ\pi 2\Gamma^2(1/n)a^{2-2/n}E_R^{1+1/n}a_H^{2/n}} \times\left[\left[(1+2\epsilon E_0)^2\sin^2\left\{(1/n)\left[\frac{\pi}{2}-\tan^{-1}\left(\frac{aE_1(1+2\epsilon E_0)}{4a_H[E_0E_R(1+\epsilon E_0)]^{1/2}}\right)\right]\right\}\right]\right]^{-1} \qquad (8)$$

where E_0 is the incident electron energy.

This satisfies quantitatively the experimental results of Young (1956), Holliday and Sternglass (1959), Glendenin (1948), Katz and Penfold (1952), Cosslett and Thomas (1964b) and the calculations of Berger and Seltzer (1964), as shown in Figure 3, where $\lambda_n^2 = \frac{1}{2}$.

From equations (7) and (8) the energy E of electrons at depth x can be simply expressed in terms of the reduced depth y=x/R:

$$E/E_0 = (1-y)^{n/(1+n)}. \qquad (9)$$

The back-scattering energy E_B of electrons at depth y is also given by

$$E_B/E_0 = (1-y)^{n/(1+n)}\left(1-\frac{y}{\cos\theta}\right)^{n/(1+n)}. \qquad (10)$$

Using the above relations of energy retardation, we can obtain the fractions of transmission, back-

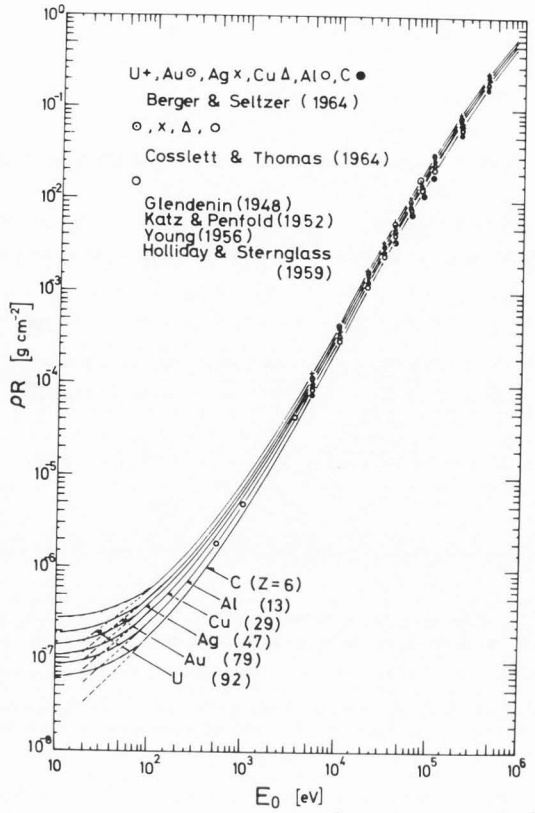

Figure 3. Energy dependence of mass-range ρR for several targets.

scattering and absorption as functions of y and n. The most probable energy dissipation depth $y_c=x_c/R$ in the diffusion model (described below in section 7) is related to the mean energy of back-scattering electrons $\bar{E}_B$, as follows:

$$\bar{E}_B/E_0=(1-y_c)^{2n/(1+n)}. \qquad (11)$$

which is in close agreement with the empirical formula of Sternglass (1954), $\bar{E}_B/E_0=0.45+2\cdot10^{-3}Z$.

4. Transmission η_T and diffusion depth y_D

The general form of variation with thickness of the fraction η_T of the incident current which is transmitted into the forward hemisphere (figure 2) obeys an exponential relation similar to the Lenard law:

$$\eta_T=i/i_0=\exp(-N\sigma x). \qquad (12)$$

The total scattering cross-section σ (equation 5) is related to the fractional range-energy relationship (9) by

$$N\sigma Ry=\gamma y/(1-y). \qquad (13)$$

When (8) is substituted into (13) and (12), η_T can be expressed as functions of γ and y:

$$\eta_T=\exp[-\gamma y/(1-y)]. \qquad (14)$$

The parameter γ involves the effects of diffusion loss due to multiple collisions for reflected electrons and energy retardation due to electronic collisions. It is related to the atomic number Z and the power of the potential function n by

$$\gamma=\Omega(n-1)(Z+1)/[n(n+1)2^{1/n}] \qquad (15)$$

which has the maximum value $[\gamma/(Z+1)]_{max}=0.083$ for the optimum value of n ($n_{opt}=2.5$), where a small fitting factor is required for Z<50 and n<1.4.

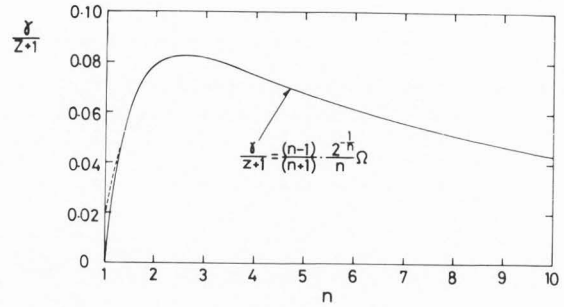

Figure 4. Energy dependence of γ/(Z+1) as a function of the screening parameter n.

Figure 4 shows the energy dependence of γ/(Z+1) as a function of the screening parameter n.

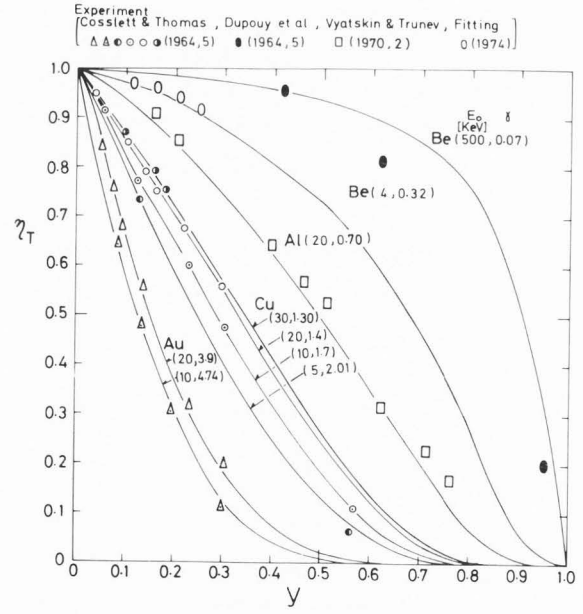

Figure 5. Transmission of electrons in several targets with the incident energies as a function of the reduced depth y. Experimental points: Cosslett and Thomas (1964a, b, 1965), Dupouy et al (1964, 1965), Fitting (1974), Vyatskin and Trunev (1970, 1972).

Figure 5 shows the variation of η_T in several target materials with the incident energies as a

function of y, which agree closely with the exprimental results by Dupouy et al (1964, 1965), Cosslett and Thomas (1964a, b, 1965), Vyatskin and Trunev (1970, 1972), Fitting (1974). From the definition of the diffusion depth x_D with the transmission function 1/e, it follows that

$$y_D = x_D/R = 1/(1+\gamma). \qquad (16)$$

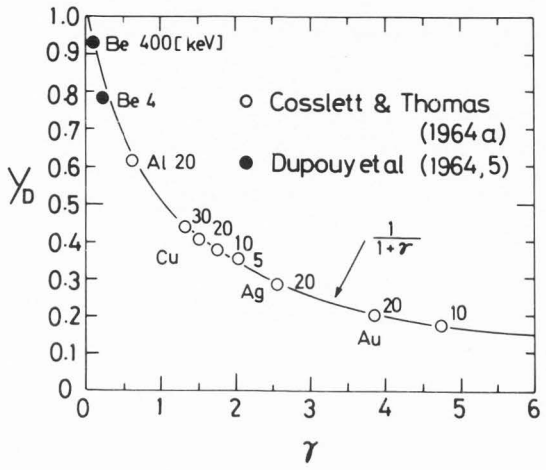

Figure 6. The reduced diffusion depth y_D as a function of γ.

This seems to be more reasonable than the previous expressions given by Meister (1958), Archard (1961) and Tomlin (1963) and it agrees well with the Monte Carlo calculations of Bishop (1965,1967). The calculated results from (16) are compared with the experimental results of Cosslett and Thomas (1964a) and Dupouy et al (1964, 1965) by using the energy dependence of γ shown in figure 4 with the atomic number and energy dependence of n.

5. Back-scattering fraction η_B

The general form of the variation of η_B with thickness (η_B is the fraction of the back-scattered electrons, which are deflected inside the limiting angle θ_0 subtended by the back-scattered radius r_B of the centre y_C of a sphere model) is shown in figure 2. η_B is assumed to have the same exponential form as η_T, but the absorption factor γ_B must be larger than γ because of diffusion loss due to multiple collisions.

Following the same Lenard law, the back-scattered electron fraction is assumed to be a form $\eta_B = \exp[-\gamma_B y/(1-y)]$, where $\gamma_B = \gamma/\Omega_1$; Ω_1 is the normalising solid angle being equal to

$$\int_0^{\pi/2} \sin\theta \, d\theta/(1+\cos\theta)^{1+1/n} = n(1-2^{-1/n}).$$

Accordingly, the effective back-scattered electron fraction inside the limiting angle θ_0, using the equation of $\cos\theta_0 = y/(1-y)$, is given by

$$\eta_B(y) = n\gamma_B \int_0^y \frac{\exp[-\gamma_B y/(1-y)]}{(1-y)^2} [(1-y)^{1/n} - 2^{-1/n}] \, dy. \qquad (17)$$

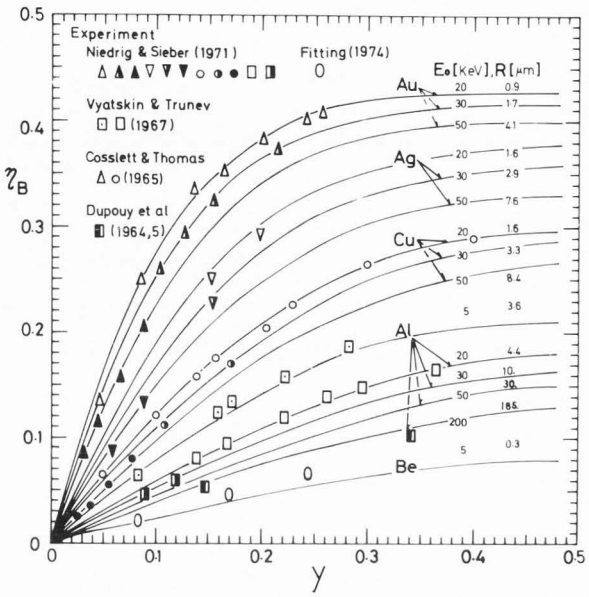

Figure 7. The fractional back-scattering η_B from several target materials with various incident energies as a function of reduced depth y. Experimental points: Niedrig and Sieber (1971), Fitting (1974), Vyatskin and Trunev (1967), Cosslett and Thomas (1965), Dupouy et al (1964, 1965).

Figure 7 shows the fractional back-scattering η_B from several target materials with various incident energies as a function of reduced depth y. The calculated results are in good agreement with experimental results of Cosslett and Thomas (1964, 1965), Dupouy et al (1964,1965), Vyatskin and Trunev (1967) and Niedrig and Sieber (1971), where the atomic density ρ is assumed to be slightly reduced by a maximum of 15%. For the special case where the depth y is small, η_B is approximately linearly proportional to the depth x as pointed out by Niedrig and Sieber (1971).

For the back-scattering coefficient as a function of angle ν of incident electron probe relative to the normal, Radzimski (1978) introduced the equation modifying the previous diffusion model by Kanaya and Okayama (1972):

$$\eta_B(\nu) = \eta_B \exp[A_0(1-\cos\nu)] \qquad (18)$$

with $A_0 = \gamma_B y_C/(1-y_C)$ where y_C is the centre of the diffusion model corresponding to the most probable energy dissipation depth. The expression seems to be very versatile because it was obtained from a model which is in a good agreement with experiments over a wide energy range ($1\text{-}10^3$keV) and atomic number range Z=3-80. Figure 8 shows the theoretical and experimental comparison of back-

scattering coefficient as a function of angle of beam incidence ν at several beam energies (Drescher et al 1970, Radzimski 1978).

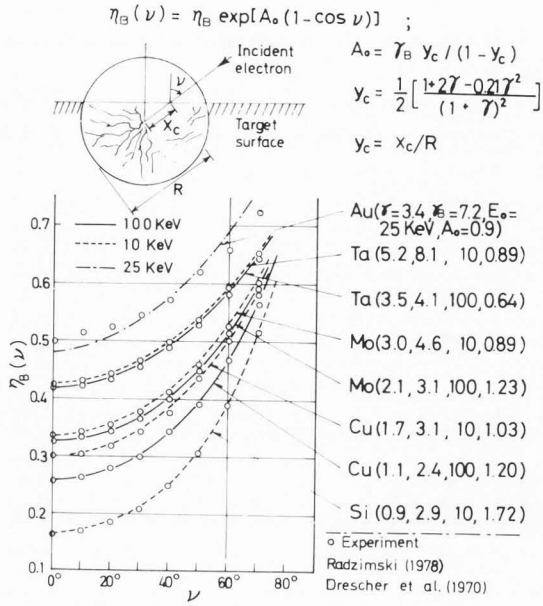

Figure 8. The back-scattering coefficient $\eta_B(\nu)$ as a function of angle ν of incident electron probe relative to the normal.

6. Absorption of electrons η_A and energy dissipation E_A

Following Cosslett and Thomas (1964a, 1965), we obtain the fraction η_A of the incident beam absorbed in a solid target from the equation

$$\eta_A = 1 - (\eta_T + \eta_B)$$

If the value of η_T is substituted from (14) and η_B from (17) into the above, η_A becomes

$$\eta_A = 1 - \left[\exp\left(-\frac{\gamma y}{1-y}\right) + n\gamma_B \int_0^y \frac{\exp[-\gamma_B y/(1-y)]}{(1-y)^2}\left[(1-y)^{1/n} - 2^{-1/n}\right] dy\right]. \quad (19)$$

The absorbed fraction calculated from (19) is in good accord with the results of Cosslett and Thomas (1965), as shown in figure 9.

The distribution of absorbed electrons at different incident energies can be represented for a given element when the normalised fraction is plotted against the reduced depth y as functions of γ and n by using the following equation:

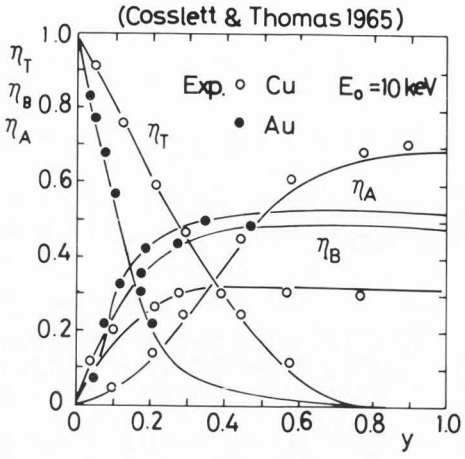

Figure 9. Relative proportions of electrons transmitted η_T, back-scattered η_B and absorbed η_A in Cu(○) and Au(●) target as a function of the reduced depth y.

$$\rho R \frac{d\eta_A}{d(\rho x)} = \frac{\gamma}{(1-y)^2} \exp\left(-\frac{\gamma y}{1-y}\right) - n\gamma_B \frac{\exp[-\gamma_B y/(1-y)]}{(1-y)^2}\left[(1-y)^{1/n} - 2^{-1/n}\right]. \quad (20)$$

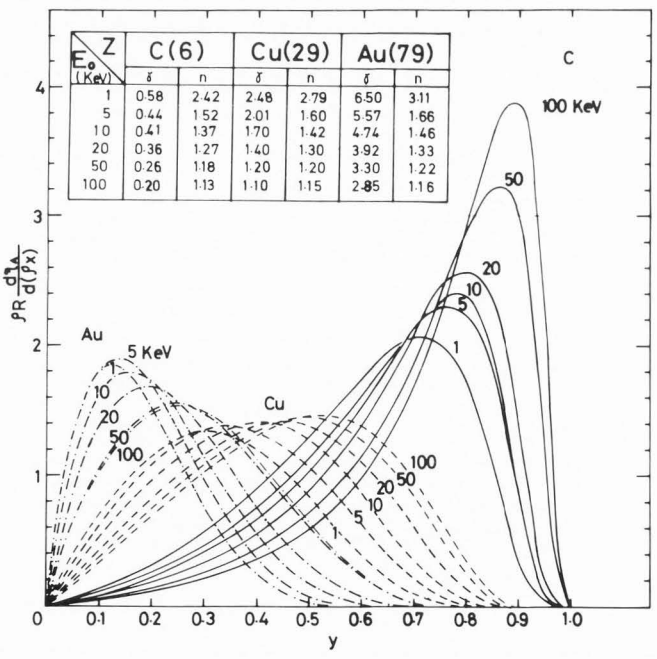

Figure 10. The distribution of absorbed electrons at different incident energies as a function of the reduced depth y.

Figure 10 shows the distribution of absorbed electrons at different incident energies as a function of the reduced depth y.

It is clearly found that the depth of absorbed electron maximum per unit mass-thickness corresponds at the diffusion depth y_D. The dissipation of energy with depth may be calculated in a similar way to the previous paper (Kanaya and Okayama 1972):

$$E_A = E_0 - \eta_T E - \eta_B \bar{E}_B$$

where E and $\bar{E}_B$ refer to the energies of transmitted and back-scattered electrons through matter, reduced by electronic collisions as given by (9) and (11), respectively.

The approximate equation of $\bar{E}_B/E_0$ in (11) is very close to the empirical relationships of Brand (1936), Kulenkampff and Rüttiger (1954), Kulenkampff and Spyra (1954), Sternglass (1954) and Klein (1968).

We deduce that, corresponding to the above equation, the energy E_A absorbed in the fractional layer of material between the surface and depth x is given by

$$\frac{E_A}{E_0} = 1 - (1-y)^{n/(1+n)} \exp\left(-\frac{\gamma y}{1-y}\right) - \eta_B(y)\frac{\bar{E}_B}{E_0}. \qquad (21)$$

Figure 11 shows the results calculated by (21) for several target materials at 10keV incident energy.

The calculated distributions of the energy explain fairly well the fact that the electron is retarded due to electronic collisions but then diverges increasingly owing to the difference in the amount of energy lost by back-scattering due to nuclear collisions. At the end of the range this is equal to the amount: $1-\eta_B(\frac{1}{2})\times[\bar{E}_B/E_0]$.

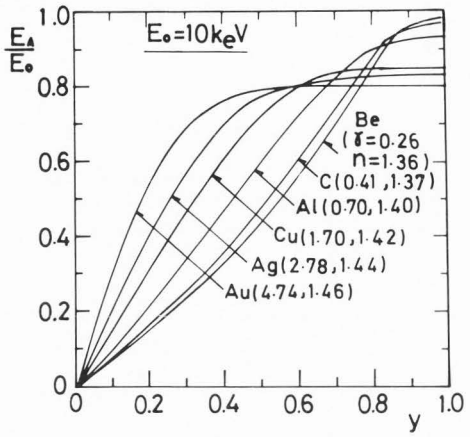

Figure 11. Fraction of energy dissipated E_A/E_0 within a given fraction of the range y in several targets at E_0=10 keV.

The reduced fraction of energy dissipated in unit mass-thickness $\rho R\, d(E_A/E_0)/d(\rho x)$ can be obtained by differentiating (21):

$$\rho R \frac{d(E_A/E_0)}{d(\rho x)} = -\frac{d\eta_T}{dy}(1-y)^{n/(1+n)} + \left(\frac{n}{1+n}\right)(1-y)^{-1/(1+n)}\eta_T - \frac{d\eta_B}{dy}\frac{\bar{E}_B}{E_0}. \qquad (22)$$

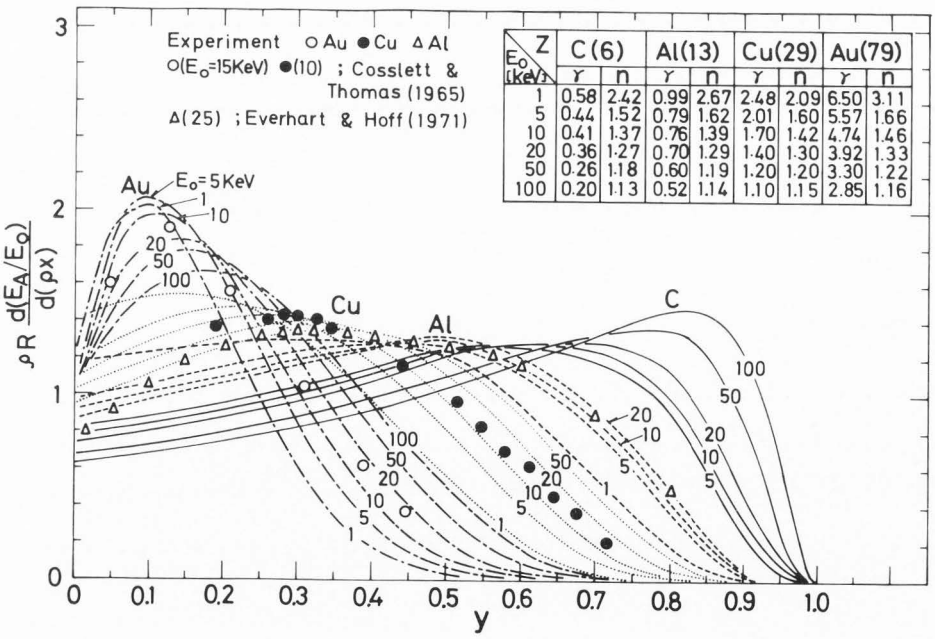

E_0 (keV) \ Z	C(6)		Al(13)		Cu(29)		Au(79)	
	γ	n	γ	n	γ	n	γ	n
1	0.58	2.42	0.99	2.67	2.48	2.09	6.50	3.11
5	0.44	1.52	0.79	1.62	2.01	1.60	5.57	1.66
10	0.41	1.37	0.76	1.39	1.70	1.42	4.74	1.46
20	0.36	1.27	0.70	1.29	1.40	1.30	3.92	1.33
50	0.26	1.18	0.60	1.19	1.20	1.20	3.30	1.22
100	0.20	1.13	0.52	1.14	1.10	1.15	2.85	1.16

Figure 12. Normalised fraction of energy dissipated in unit mass-thickness as a function of the reduced depth y for several target materials at different incident energies.

Figure 12 shows the result calculated by (22) for several target materials at different incident energies. The distributions for the two elements Cu and Au are very similar at the same incident energy to curves of Cosslett and Thomas (1964a,b, 1965).

In the figure the peak position for heavy elements ($\gamma>1$) corresponds to the depth of energy dissipation maximum experimentally obtained by Cosslett and Thomas (1965). The theoretical and experimental distributions show quantitative agreement, but the experimental peak value is located at almost the reduced depth for light elements ($\gamma<1$).

7. Diffusion model

On the basis of the modified Bethe energy-loss theory, Kanaya and Okayama (1972) proposed the so-called 'modified diffusion model' of a sphere in which electrons move equally in all directions from the depth of maximum energy dissipation depth x_E and in such a way that their overall paths are equal to the difference of full range $R-x_E$.

For a high atomic number this model agrees fairly well with the photograph of electron glow published by Ehrenberg and Franks (1953) and Ehrenberg and King (1963), and by Brewer (1971) using photoresist layers with electron beam exposure techniques, but for a low atomic number at high-energy range it does not agree because back-scattered electrons reaching the surface in their original directions vanish. The model disregards electrons undergoing large-angle elastic reflection between the surface and the depth of complete diffusion.

The back-scattering range r_B is given by

$$y_B = r_B/R, \qquad r_B = cR\gamma/(1+\gamma) \tag{23}$$

where the best fit is obtained by taking c=1.1 on an empirical basis.

The most probable energy dissipation depth x_C can be obtained by a simple geometric relation

$$y_C = x_C/R = \tfrac{1}{2}\left(1-\frac{c^2\gamma^2}{(1+\gamma)^2}\right) = \frac{(1+2\gamma-0{\cdot}21\gamma^2)}{2(1+\gamma)^2}. \tag{24}$$

Then the back-scattering coefficient r can be obtained from the following equation:

$$r = \frac{1}{4\pi}\int_0^{\theta_0} 2\pi \sin\theta \, d\theta = \tfrac{1}{2}(1-\cos\theta_0) \tag{25}$$

with

$$\tan\theta_0 = r_B/x_C = \frac{2{\cdot}2\,\gamma(1+\gamma)}{1+2\gamma-0{\cdot}21\gamma^2}. \tag{26}$$

Figure 13 shows the comparison of the present diffusion model's parameters of y_D, y_E, y_C, y_B and r compared with theoretical values calculated by (20), (22), (24), (23) and (25) respectively. As shown in Figure 4, the parameter γ by (15) has the peak value under the optimum condition of $n_{opt} = 2.5$ (corresponds to E_0 = 700~2000 eV for Z from 1 to 10).

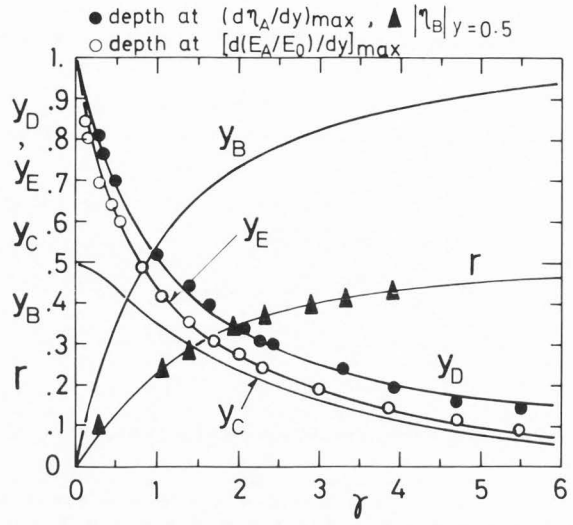

Figure 13. The comparison of the present diffusion model's parameters of y_D, y_E, y_C, y_B and r compared with the theoretical values calculated by (20), (22), (24), (23) and (25), respectively.

The important parameters of diffusion depth y_D and y_E are obtained using a diffusion model:

$$y_D = 1/(1+\gamma) \tag{27}$$

$$y_E = y_D - [\gamma/(1+\gamma)](y_D - y_C). \tag{28}$$

Figure 14 shows the energy dependence of the back-scattering coefficient $[\eta_B]_{Y=1/2}$ =r which has the maximum values of r_{max} and the corresponding optimum energies for various target materials, which are substantially close to the experimental results by Fitting (1974), Wright and Trump (1962), and others.

Figure 15 represents the present diffusion models for several target materials, where the broken curves are the original models.

8. Conclusions

(1) Results of interest in connection with the fundamental theory of electron scattering such as mass-range, transmission, diffusion depth, back-scattering, energy-loss and maximum energy-loss depth, are consistently expressed in normalised form with the reduced depth y as a function of the parameter which is derived as a function of both the incident energy and the atomic number.

(2) A diffusion model represented by a hemisphere whose centre is located at the most probable

Figure 14. Energy dependence of the back-scattering coefficient r which has the maximum value of r_{max} and the corresponding optimum energies E_{opt} for several target materials. Experimental results with △ Au, ○ Ag, ◇ Ge, □ Cu, ▼ Al, ✕ C, ● Be: Kanter 1957 (△○); Wright and Trump 1962 (△□▼●); Weinryb and Philibert 1964 (▼●); Cosslett and Thomas 1965 (△□); Verdier and Arnal 1968,69 (○□▼✕); Ebert et al. 1969 (○□▼✕); Bronshtein and Fraiman 1969 (△○▼●); Niedrig and Sieber 1971 (△○□▼); Fitting 1974 (○◇▼●).

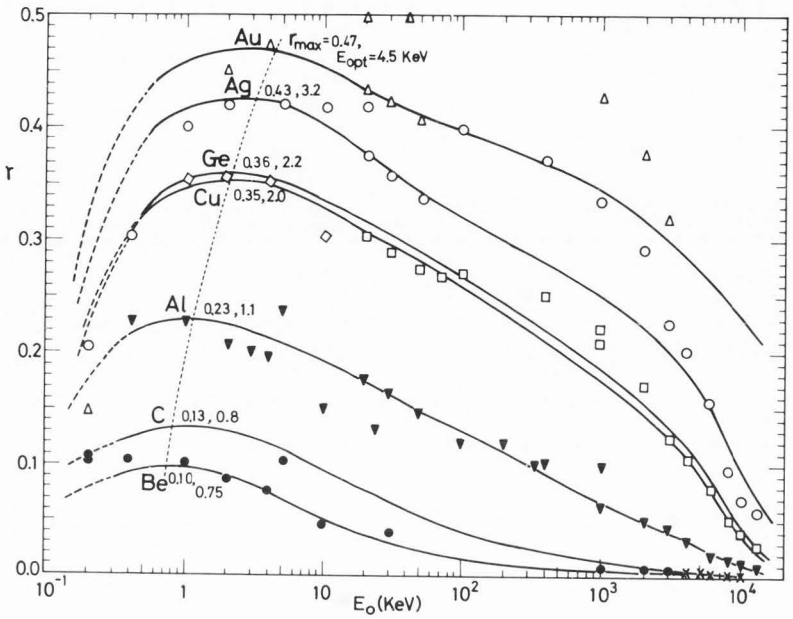

Figure 15. Representation of the present diffusion models for several target materials at E =10 keV, where the broken curves are the original models.

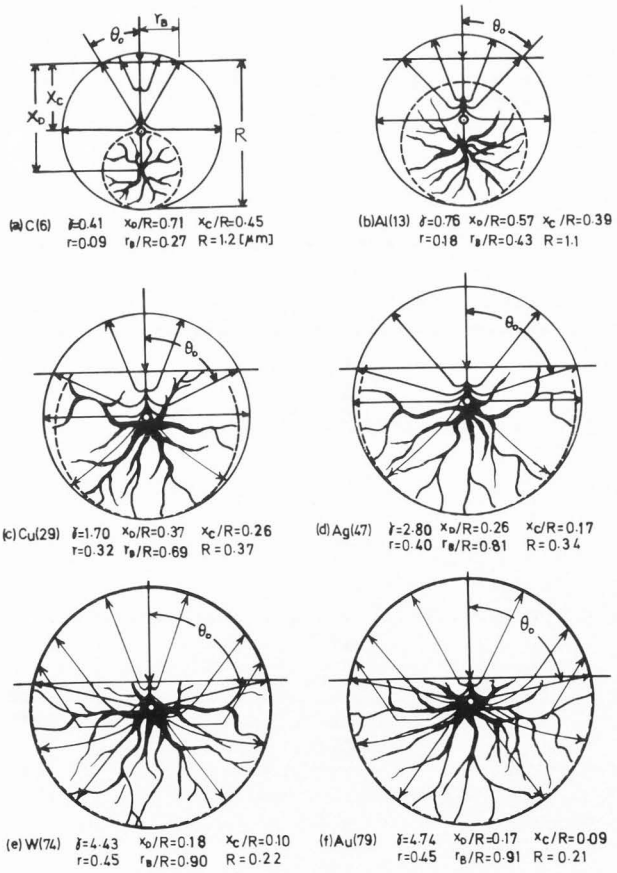

energy dissipation depth y_C, related to the diffusion depth y_D and the maximum energy dissipation depth y_E, is found to agree well with the empirical data.

(3) In a similar way to the 'yield-energy' relationship of the secondary electron emission, the back-scattering coefficient increases as the incident energy decreases and the maximum value again decreases and the optimum energy giving the maxima range from 500 eV to 5 keV, corresponding to the atomic numbers of target materials from Z=1 to 100, respectively.

Ⅱ The Energy Dependence of Secondary Emission Based on the Range-Energy Retardation Power Formula

1. Introduction

Many attempts have been made to explain secondary electron emission induced by electron bombardment qualitatively and quantitatively since the work of Austin and Starke (1902). Recently, considerable interest has arisen in the use of secondary electron emission from a solid target by the bombardment of a finely focused 30keV highly accelerated beam of electrons as in scanning electron microscopes. The quantitative analysis of secondary electron images in scanning electron microscopes requires the exact values of yield, the escape depth of secondary electrons, and the contribution of back-scattered electrons within a solid target.

Based on the assumption of two mechanisms in the secondary electron emission process (the production and escape mechanisms of secondary electrons), there have been some theories of the secondary emission, such as a free-electron theory of Baroody (1950), cascade theory of Wolff (1954), and quantum theory of the production of secondaries (Fröhlich 1932, Wooldridge 1939, Dekker and van der Ziel 1952, Marshall 1952, van der Ziel 1953, Baroody 1953, 1956). In addition, the semi-empirical theories based on the electron range-energy power-law (the Thomson-Whiddington law) have been presented by Salow (1940), Bruining & De Boer (1938), Bruining (1954), Jonker(1952,1954), Lye and Dekker (1957), and Dekker (1958).

In the recent work, Kanaya and Kawakatsu (1972) and Dionne (1973, 1975) have developed the theory of secondaries by the generalised power law concerning the energy loss of electrons penetrating into a solid target making use of range measurements by Glendenin (1948), Katz and Penfold (1952), Lane and Zaffarano (1954), Young (1956), Holliday and Sternglass (1959), and by Cosslett and Thomas(1964).

An attempt (Ono and Kanaya, 1979) has been made to present a sufficient solution of the secondary electron yield of metals and semiconductor compounds except insulators, by applying the free-electron scattering theory to the absorption of secondary electrons generated within a solid target. For insulators, Kanaya et al(1978) have presented a sufficient solution of the high yield and an explanation of the different yield appearing in integral multiples, combining the free-electron scattering theory with the plasmon theory.

By using the potential function of the power and exponential forms as a function of a modified screened atomic radius for electron scattering (Kanaya and Ono 1976), the range energy relationship of $R=(E_0/E_R)^{1+1/n}/c_0$, with an incident energy E_0 of between 1 keV and 1 MeV, is used as a fundamental equation, where n indicates the degree of screening (n goes from 1 to ∞ as the accelerating voltage decreases), E_R is the Rydberg energy and c_0 the range-energy coefficient of the primary beam.

The purely classical empirical theory (Bruining 1954, Jonker 1952, 1954, Lye and Dekker 1957, Kanaya and Kawakatsu 1972) is developed by the power law concerning the energy loss. Also, by using the absorption law of Lenard type and the assumption that the distribution of secondary electrons with energies below 50 eV produced by primary electrons within the target is isotropic, the universal yield-energy curve is deduced. It is shown that the absorption coefficient of secondary electrons involved in the Lenard law relates with the suitably averaged ionisation loss, since the energy of secondary electrons produced by the first collision of primary electrons with the target is very small, i.e. E_S = 100-200 eV (Rauth and Simpson 1964).

Since the resulting maximum yield δ_m and the energy E_m mainly depend on the range-energy coefficient of the primary beam c_0 and the absorption coefficient α, these can be given as functions of ionisation energy I, back-scattering coefficient r and the atomic number Z.

2. Absorption coefficient α and escape depth x_α

The absorption coefficient α of secondary electrons generated within the solid target is a most significant factor in quantitative evaluation of the maximum yield δ_m which is, in practice, measured with its corresponding incident energy E_m.

Suppose that the secondary electrons are distributed following the Lenard (1918) law after their dislodgement and satisfy the special case n=4 of the power law (eq. 2) in the first collision.

Since their energy of most probable ionisation loss in the first collision is very low (E_S=100-200 eV, Rauth and Simpson 1964) compared with the primary energy $E_0 \geqslant 5$ keV, the transmission fraction of secondaries is given by

$$i_s/i_0=\exp(-N\sigma_i x)=\exp(-\alpha x) \qquad (1)$$

where i_S is the secondary emission current, i_0 the primary beam current, N the number of atoms per unit volume, and σ_i is the total scattering cross-section due to the loss of secondary electrons.

Then, the total cross-section σ_i (for secondary emission) (Kanaya and Ono 1976) is given by

$$\sigma_i=\lambda_\infty^2 4\pi Z a^2 (E_R/E_s)\ln\left(\frac{4E_s}{I}\right) \qquad (2)$$

where λ_∞^2 is the constant determined empirically, $a=0.77a_H Z^{-1/6}$ Å the screened atomic radius, a_H the Bohr radius of hydrogen, and $n=\infty$ is assumed because the energy of secondary electrons is very low. The ionisation energy E_S is ranged between 92 and 235 eV for Al, Cu, Si and Au (Rauth and Simpson 1964), and it can be approximated as

$$E_s=n_s I \qquad (3)$$

where I is the first ionisation energy and n_S, the constant, is taken to be n_S=20.

Accordingly, the most probable escape depth of secondary electrons x_α, in a similar manner to the diffusion model by Archard (1961), from i_S/i_0 1/e, is given by

$$x_\alpha=1/\alpha=2{\cdot}67\,A_0 I/\rho Z^{2/3}\ (\text{Å}) \qquad (4)$$

where λ_∞^2=0.1 is used. A_0 the atomic weight and ρ the density. Figure 1 shows the escape depth of secondary electrons x_α as a function of atomic number Z, which is in good agreement with Seiler's (1967) data.

3. Secondary yield due to primary and back-scattered electrons

According to the elementary theory, the number of secondary electrons ejected from the target increases in proportion to the energy loss, they are isotropically distributed in the solid target, and are emitted from the surface following the absorption law of Lenard type after their dislodgement.

The analytical treatments, as well as Monte-Carlo calculations, are very useful to evaluate

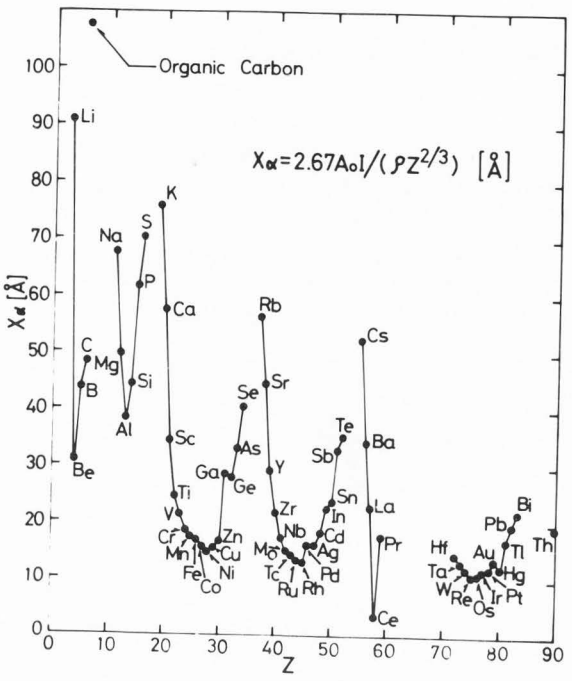

Figure 1. The escape depth of secondary electrons x_α as a function of atomic number Z.

the secondary electron emission mechanisms from metals by electron beam bombardment, which have been developed by Jonker (1952,1954) and Lye and Dekker (1957) and others, and Reimer (1968), Shimizu and Murata (1971), Shimizu (1974), Ganachaud and Cailler (1975a, b), Ganachaud (1977), and Pillon et al (1977), respectively.

Suppose an incident electron beam falls perpendicularly on a solid target. The number of secondary electrons released is proportional to the electron energy loss dE/dx. They arrive at the surface by travelling a distance $\ell = x/\cos\theta$ through the material, and the secondary yield is given by Jonker (1952, 1954) and Kanaya and Kawakatsu (1972) as

$$\delta = \frac{K}{2}\int_0^R \frac{d(E/E_R)}{dx}\int_0^{\pi/2} \exp\left(-\frac{\alpha x}{\cos\theta}\right)\sin\theta\, d\theta\, dx \qquad (5)$$

where K is the constant depending on the penetration of electrons.

By using the range-energy relationship and the resulting energy retardation formula (Kanaya and Ono 1976), the secondary yield due to primary electrons δ_p can be given by

$$\delta_p = \frac{K}{2}\left(\frac{c_0}{\alpha}\right)^{n/(1+n)}\int_0^1 \frac{n}{1+n} A^{n/(1+n)}(1-y)^{-1/(1+n)}$$

$$[\exp(-Ay) + AyE_1(-Ay)]\, dy \qquad (6)$$

where $A = \alpha R = (\alpha/c_0)(E_0/E_R)^{1+1/n}$ and

$$E_1(-x) = -\int_x^\infty \exp(-t)/t\, dt$$

is the exponential integral function.

Most incident electrons are scattered through small angles as they interact with atoms. As the electron penetration increases deeply, the primary beam spreads in a Gaussian manner, as shown in a previous paper of diffusion model (Kanaya and Ono 1978). Consideration of the back-scattered electrons becomes especially important because their maxima ranged between 500 and 2000eV. According to Kanter (1961) the back-scattered electrons from the interior of the material follow a cosine distribution. Therefore the rate of energy loss and the path lengths of back-scattered electrons in the region of secondary escape are large compared with those of the incoming primaries. Thus the secondary electron yield cannot be disregarded when the back-scattering coefficient η_B is relatively large.

Consider the production of secondary electrons by back-scattered electrons δ_B is given by

$$\delta_B = \eta_B\left(\frac{K}{2}\right)\left(\frac{c_0}{\alpha}\right)^{n/(1+n)}\int_0^{1/2}\left(\frac{2n}{1+n}\right)(1-y)^{(n-1)/(n+1)}$$

$$\times A^{n/(1+n)}[\exp(-Ay) + AyE_1(-Ay)]\, dy. \qquad (7)$$

The total secondary yield δ is then considered to be the sum of secondary electrons due to primary electrons and secondary electrons due to back-scattered electrons:

$$\delta = \delta_p + \delta_B. \qquad (8)$$

It can be simply expressed by

$$\delta/[(K/2)(c_0/\alpha)^{n/(1+n)}] = f_p(A) + \eta_B f_B(A) \qquad (9)$$

in which $f_p(A)$ and $f_B(A)$ are the integrations in equations (6) and (7), respectively, and have maxima as shown in Kanaya et al (1978).

Accordingly, the value of total yield normalised by the maximum yield δ/δ_m can be obtained as a function of E/E_m:

$$\delta/\delta_m = [f_p(A) + \eta_B f_B(A)]/[f_p(A) + \eta_B f_B(A)]_{max} \qquad (10)$$

for $E/E_m = (A/A_m)^{n/(1+n)}$. For the sake of simplicity for the calculation, it can be numerically approximated as

$$[f_p(A) + \eta_B f_B(A)]_{max} = 0{\cdot}365\,(1 + 1{\cdot}26\, r) \qquad (11)$$

and

$$A_m = (1 + 5r^2) \qquad (12)$$

where the back-scattering coefficient $r = [\eta_B]_{y=1/2}$, where η_B is the back-scattering fraction with depth y=x/R, is used from the diffusion model (Kanaya and Ono 1978) as

$$r = \tfrac{1}{2}(1 - \cos\theta_0) \qquad (13)$$

with

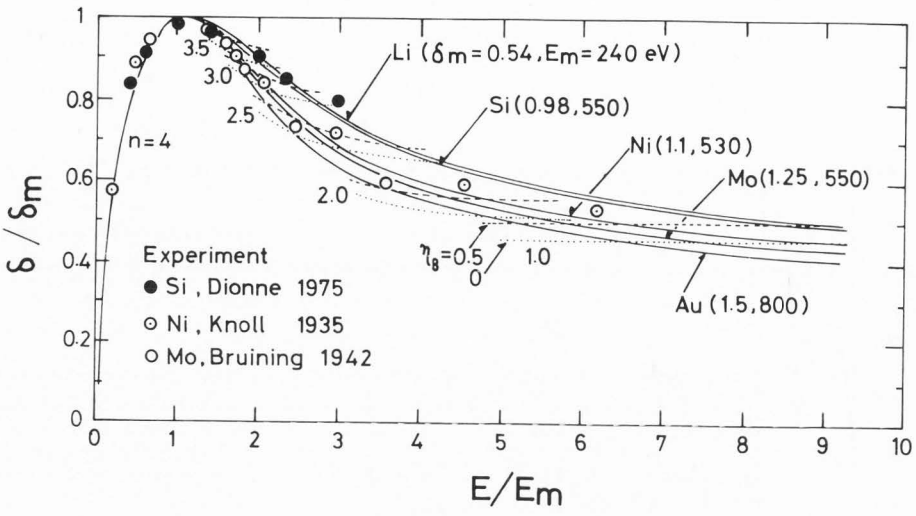

Figure 2. The theoretical and experimental comparison of the universal yield-energy curve for the energy-dependent parameter n.

$$\left.\begin{aligned}
&\tan\theta_0=\frac{2\cdot2\gamma}{1+2\gamma-0\cdot21\gamma^2}\\
&\gamma=\Omega(n-1)(Z+1)/[n(n+1)2^{1/n}]\\
&\Omega=\tfrac{1}{3}\left(\int_0^{\pi/2}d\Omega+\frac{1}{2!}\int_{\pi/2}^{3\pi/4}d\Omega+\frac{1}{3!}\int_{\pi/2}^{5\pi/6}d\Omega\right)\\
&d\Omega=\sin\theta\,d\theta/(1+\cos\theta)^{1+1/n}
\end{aligned}\right\}\quad(13)$$

which is very close to the empirical result by Seiler (1967).

Figure 2 represents the theoretical and experimental comparison of the universal yield-energy curve for the energy-dependent parameter n, where the upper limit of the curve corresponds to the light element of the target and lower limit to the heavy element, respectively, and the yield increases as the back-scattering coefficient η_B increases. The energy and back-scattering dependence of the universal yield-energy curves are in good agreement with the experiments of Si, Ni and Mo.

4. Quantitative characteristics of secondary yield

The value of the incident energy E_m for which the maximum yield occurs is related to α and c_0:

$$(E_m/E_R)^{1+1/n}=(c_0/\alpha)A_m=(c_0/\alpha)(1+5r^2)\qquad(14)$$

where A_m is approximately given by equation (12) related with the back-scattering coefficient r. From equations (6) and (7), for the assumption n=4 in the first collision, which corresponds to the energy E_m=500-2000 eV, and the empirical data for Au: E_m = 800 eV, r= 0.45, I=9.2 eV, then the characteristic energy E_m is simply approximated as

$$E_m=57\cdot9Z^{1/15}I^{4/5}(1+5r^2)^{4/5}\ (\mathrm{eV}).\qquad(15)$$

On the other hand, the maximum yield δ_m is given by

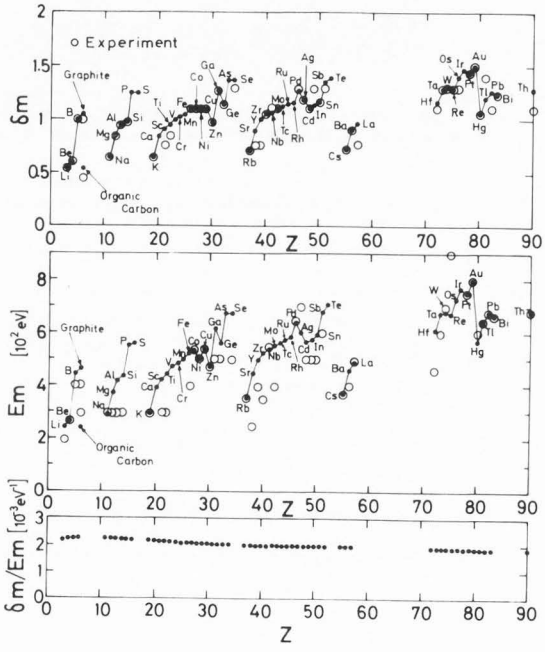

Figure 3. Comparison of the maximum yield of secondary electrons δ_m, the corresponding primary energy E_m and the ratio calculated by the range-energy retardation power formula with experiment.

$$\delta_m=\frac{K}{2}(c_0/\alpha)^{n/(1+n)}\,0\cdot365\,(1+1\cdot26\,r).\qquad(16)$$

According to the empirical relationship δ_m/E_m leads to

$$\frac{\delta_m}{E_m}=\left(\frac{K}{2}\right)\frac{0\cdot365\,(1+1\cdot26\,r)}{E_R\,(1+5\,r^2)^{4/5}}$$

$$\simeq K_0\,\frac{(1+1\cdot26\,r)}{(1+5\,r^2)^{4/5}}\qquad(17)$$

where $K_0=2.1\cdot10^{-3}(eV^{-1})$ is closely fitted to $\delta_m=1.5$ for Au.

Then, the maximum yield δ_m is empirically given by

$$\delta_m=0{\cdot}12\,Z^{1/15}\,I^{4/5}\,(1+1{\cdot}26\,r). \qquad (18)$$

Figure 3 shows the above calculated results, compared with experimental results (Dekker 1958, Seiler 1967, Kollath 1956, von Ardenne 1959, Gobrecht and Speer 1953), in which experimental points are made to accord with calculated results when the differences are within 10%. The physical properties of materials used in calculation is shown in table 1, in which some data (as shown in parentheses) for the first ionisation energy is corrected by the Smithsonian Physical Tables(1954) as follows; for B, Al, Ga, In, Tl the corrected value is the first ionisation energy plus 1-2 eV, but for He, Be, Mg, Zn, Cd, Hg the first ionisation energy minus 2-3 eV, and for the organic carbon the resonance potential of graphitised carbon is adopted.

For semiconducting compounds of the composition $(Z_1)_p(Z_2)_q$ in the similar treatment of Hohn and Niedrig (1972) it is assumed that the secondary yield of compounds is proportional to the atomic composition and the following relationship can be derived:

Table 1. Maximum yield and energy of secondary electrons, and atomic properties of target materials.

Atom	Z	I(eV)	r	E_m (eV) (expt)	δ_m (expt)	δ_m/E_m (10^{-3} eV^{-1})
Li	3	5·4	0·07	240 (100–200)	0·54 (0·47–0·55)	2·23
Be	4	6·0 (9·27)	0·08	270 (200–300)	0·61 (0·5–0·75)	2·24
B	5	10·9 (8·28)	0·08	450 (400)	1·0 (1·0)	2·24
Graphite	6	11·2	0·10	470 (300–400)	1·1 (0·9–1·0)	2·26
Organic C	6	4·9	0·10	240 (300)	0·55 (0·45)	2·27
Na	11	5·2	0·19	290 (300)	0·66 (0·65)	2·27
Mg	12	7·0 (7·61)	0·20	370 (300)	0·84 (0·8–0·9)	2·27
Al	13	8·0 (5·95)	0·20	420 (250–300)	0·95 (0·9–1·0)	2·26
Si	14	8·1	0·22	430 (300)	0·98 (0·9–1·1)	2·25
P	15	10·6	0·23	550	1·24	2·24
S	16	10·4	0·25	560	1·24	2·22
K	19	4·4	0·28	300 (300)	0·65 (0·55–0·69)	2·18
Ca	20	6·1	0·28	390	0·85	2·17
Sc	21	6·6	0·29	430 (300)	0·92 (0·75)	2·16
Ti	22	6·8	0·30	440 (300)	0·95 (0·75–0·85)	2·14
V	23	7·2	0·31	470	1·01	2·13
Cr	24	7·3	0·32	480	1·02	2·11
Mn	25	7·4	0·32	500	1·04	2·10
Fe	26	7·8	0·33	520 (400)	1·10 (1·1–1·32)	2·11
Co	27	7·8	0·33	530 (400–600)	1·10 (0·9–1·2)	2·08
Ni	28	7·6	0·34	530 (500–550)	1·10 (1·0–1·3)	2·07
Cu	29	7·7	0·34	530 (500–600)	1·11 (1·05–1·3)	2·08
Zn	30	6·5 (9·36)	0·35	470 (200–500)	0·97 (0·9–1·1)	2·06
Ga	31	9·0 (6·0)	0·35	610 (300–500)	1·27 (1·3)	2·07
Ge	32	7·9	0·35	560 (300–500)	1·15 (0·95–1·2)	2·06
As	33	9·8	0·36	670	1·37	2·04
Se	34	9·7	0·36	670 (400–500)	1·36 (0·6–1·3)	2·04
Rb	37	4·2	0·37	350 (350)	0·71 (0·7–0·85)	2·02
Sr	38	5·6	0·37	440 (250)	0·90 (0·75)	2·02
Y	39	6·4	0·38	500 (350–400)	1·00 (0·75)	2·00
Zr	40	6·8	0·38	530 (350)	1·06 (0·9–1·1)	2·02
Nb	41	6·9	0·38	540 (550)	1·07 (1·1–1·2)	1·99
Mo	42	7·1	0·38	550 (400)	1·10 (1·1–1·2)	2·00
Tc	43	7·2	0·39	560	1·12	1·99
Ru	44	7·4	0·39	580	1·15	2·00
Rh	45	7·4	0·39	580	1·15	1·98
Pd	46	8·3	0·39	640 (650)	1·27 (1·3)	1·99
Ag	47	7·6	0·39	600 (700)	1·18 (1·2–1·4)	1·97
Cd	48	7·0 (8·99)	0·40	560 (450–500)	1·11 (0·9–1·1)	1·97
In	49	7·1 (5·79)	0·40	570 (500)	1·13 (1·3–1·4)	1·98
Sn	50	7·3	0·40	590 (500)	1·16 (1·1–1·35)	1·97
Sb	51	8·7	0·40	680 (600)	1·34 (1·2–1·3)	1·97
Te	52	9·0	0·41	700	1·38	1·96
Cs	55	4·0	0·41	370 (300–400)	0·72 (0·5–0·76)	1·95
Ba	56	5·2	0·41	460 (400)	0·90 (0·65–0·9)	1·95
La	57	5·6	0·41	490 (500)	0·95 (0·80)	1·94
Hf	72	7·0	0·43	610 (460)	1·17 (1·1)	1·91
Ta	73	7·9	0·43	670 (600)	1·29 (1·1–1·35)	1·91
W	74	8·0	0·43	680 (700)	1·31 (1·05–1·4)	1·92
Re	75	7·9	0·43	680 (900)	1·29 (1·30)	1·91
Os	76	8·7	0·43	730	1·40 (1·30)	1·92
Ir	77	9·2	0·43	770	1·47	1·92
Pt	78	9·0	0·43	760 (700–750)	1·44 (1·35–1·7)	1·91
Au	79	9·2	0·45	800 (700–875)	1·50 (1·2–1·58)	1·88
Hg	80	6·0 (10·43)	0·45	570 (600)	1·06 (1·05)	1·86
Tl	81	7·0 (6·1)	0·45	640 (650)	1·21 (1·4)	1·88
Pb	82	7·5	0·45	680 (500–700)	1·27 (1·1)	1·86
Bi	83	7·3	0·45	670 (500–700)	1·25 (1·2)	1·87
Th	90	7·5	0·45	690 (600–800)	1·28 (1·1)	1·87

Physical data refer to American Institute of Physics Handbook(Dieke 1963, Frederikse 1963).

$$\delta_m=\frac{1}{p+q}\,(p\,\delta_{1m}+q\,\delta_{2m})$$

and

$$E_m=\frac{1}{p+q}\,(p\,E_{1m}+q\,E_{2m})\ (\text{eV})$$

where Z_1 and Z_2 are the atomic numbers of the constituent elements in the compound, respectively. Table 2 shows the maximum yield and the primary energy of secondary electrons of semiconducting compounds, compared with experiments, which are calculated by the above procedures.

Table 2. Maximum yield and energy of secondary electrons of semiconducting compounds, and their atomic properties.

Material	I(eV)	r	E_m (eV) (expt)	δ_m (expt)	δ_m/E_m (10^{-3} eV^{-1})
Cu_2O	7·7 (Cu)	0·34 (Cu)	550	1·18	2·14
	13·6 (O)	0·15 (O)	(500)	(1·19–1·25)	
PbS	7·5 (Pb)	0·45 (Pb)	620	1·26	2·03
	10·4 (S)	0·25 (S)	(500)	(1·2)	
MoS_2	7·1 (Mo)	0·38 (Mo)	560	1·19	2·14
	10·4 (S)	0·25 (S)		(1·10)	
MoO_2	7·1 (Mo)	0·38 (Mo)	570	1·25	2·18
	13·6 (O)	0·15 (O)	(450)	(1·09–1·33)	
WS_2	8·0 (W)	0·43 (W)	600	1·26	2·10
	10·4 (S)	0·25 (S)		(0·96–1·04)	
Ag_2O	7·6 (Ag)	0·39 (Ag)	590	1·23	2·07
	13·6 (O)	0·15 (O)	(500)	(0·98–1·18)	

5. Angular distribution of secondary electron emission

The angular distribution of the emitted electrons can be obtained by the aid of the calculation of sect. 3. Let a part of the secondary electrons dislodged in a part of dx on the path of the primaries travel to the surface along the line l along a path at angle θ. To reach the surface the secondaries must travel a distance $l=x/\cos\theta$. Then, the secondary yield $\delta_p(\theta)$ due to primary electrons emerging in the direction l under an angle θ leads to

$$\delta_p(\theta)=(K/2)\int_0^R \left(\frac{dE/E_R}{dx}\right)\exp\left(\frac{-\alpha x}{\cos\theta}\right)dx. \qquad (19)$$

Then, $\delta_p(\theta)$, and $\delta_B(\theta)$ due to back-scattered electrons can be written as

$$\delta_p(\theta)=(K/2)\left(\frac{c_0}{\alpha\cos\theta}\right)^{n/(1+n)}\int_1^0 \frac{n}{1+n}(1-y)^{-1/(1+n)}A_\theta^{n/(1+n)}\exp(-A_\theta y)\,dy \qquad (20)$$

$$\delta_B(\theta)=(K/2)\eta_B\left(\frac{c_0}{\alpha\cos\theta}\right)^{n/(1+n)}\int_{1/2}^0 \frac{2n}{1+n}(1-y)^{(n-1)/(n+1)}A_\theta^{n/(1+n)}\exp(-A_\theta y)\,dy \qquad (21)$$

where

$$A_\theta=A/\cos\theta=(\alpha/c_0)(E_0/E_R)^{1+1/n}/\cos\theta.$$

6. Effect of incident angle on secondary yield

The calculation of $\delta(\nu)$ can be extended to the case where the primary beam strikes the surface at an angle ν to the normal. Secondary electrons dislodged at a point x on the path of the primary electrons in the material will then be located at a distance $x\cos\nu$ from the surface, so that in the above calculation x has to be replaced by $x\cos\nu$ and the absorption factor becomes $\exp(-\alpha x\cos\nu/\cos\theta)$.

If the new variable $A_\nu=(\alpha\cos(\nu)/c_0)(E_0/E_R)^{1+1/n}$ is substituted in equation (9), $\delta(\nu)$ is given by

$$\delta(\nu)=(K/2)\left(\frac{c_0}{\alpha\cos\nu}\right)^{n/(1+n)}[f_p(A_\nu)+\eta_B f_B(A_\nu)]. \qquad (22)$$

Then, the secondary emission yield maximum $\delta_m(\nu)$ and the energy for $E_m(\nu)$ normalised as a function of the incident angle ν of primary electrons become

$$\frac{\delta_m(\nu)}{\delta_m}=\frac{E_m(\nu)}{E_m}=(\cos\nu)^{-n/(1+n)}. \qquad (23)$$

In scanning electron microscopes, as shown by Oatley et al (1965), an oblique illumination is very effective to collect secondary electrons satisfactorily, since too small secondary electron currents are subject to statistical quantum noise.

7. Secondary electron emission yield transmitted

For a thin specimen with thickness d less than the penetration range R, the secondary electrons due to the electron beam bombardment on to the specimen are ejected from both surfaces, as has been recently investigated by Llacer (1968) and Jahrreiss (1964). The secondary electrons transmitted through the material behave in a manner similar to that described in the section 3. Then, from equation (6) the transmitted secondary yield δ_t is given by

$$\delta_t=(K/2)(c_0/\alpha)^{n/(1+n)}\int_0^{y_d}\frac{n}{1+n}(1-y)^{-1/(1+n)}A^{n/(1+n)}\{\exp(-A(y_d-y))+A(y_d-y)E_1[-A(y_d-y)]\}\,dy \qquad (24)$$

where $y_d=d/R$. And, moreover, the secondary yield δ_s from the surface of target for thin specimen with thickness d can be given by

$$\delta_s=(K/2)(c_0/\alpha)^{n/(1+n)}\int_0^{y_d}\frac{n}{1+n}(1-y)^{-1/(1+n)}A^{n/(1+n)}[\exp(-Ay)+AyE_1(-Ay)]\,dy. \qquad (25)$$

Figure 4 shows the comparison with the secondary yield δ_t and δ_s for the specimen thickness d=50 and 100 Å, where the parameters, n and c_0 are given by equations I-(2) and I-(8), respectively, and as a function of A; $A=(\alpha/c_0)(E_0/E_R)^{1+1/n}$. It is found that both

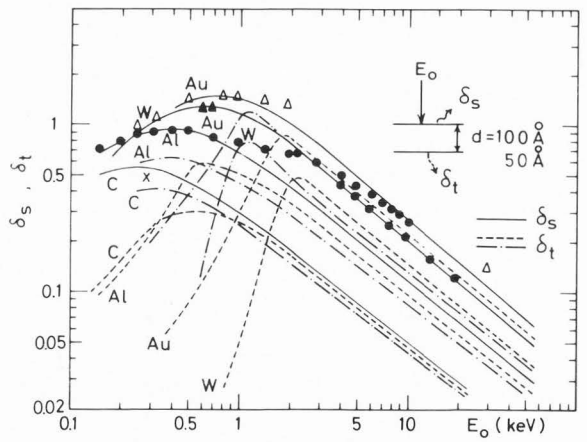

Figure 4. A comparison between the secondary yields δ_t and δ_s for the thickness d=50 and 100 Å. Experiments of δ for thick targets (Δ Au; ▲ W; ● Al; x C, by Kollath 1956, Kanter 1961, Wittry 1966, Thomas and Pattinson 1970, Shimizu 1974) are plotted for a comparison with the theoretical curves of δ_t(d=100 Å). Calculated curves are drawn by ——— δ_s for d=100 Å, ---- δ_t(d=100 Å), and —— · —— δ_t(d=50 Å). δ_s(d=50 Å) is smaller about 5-10% than the value of δ_s(d=100 Å) for $E_0\lesssim 2$ keV. For $E_0\gtrsim 5$ keV the difference between δ_s(d=100 Å) and δ_s(d=50 Å) is very small.

yields of δ_t and δ_s have maxima as a function of the incident energy depending on the penetration range and escape depth, which can be successfully interpreted by using A_m in equation (12). In the case of a gold target, for example, $A_m=2$ calculated by equation (12) with r= 0.45 is in good agreement with the calculated ratio R/x_{α_o} $(=A_m=\alpha R)=2$; for this target, R=30 Å and x_α=14 Å at E_m=800 eV. If the specimen for a scanning electron microscope (SEM) is thin enough and can be mounted to collect secondary electrons from both sides of the specimen surface, it may be a useful method for increasing the number of secondary electrons or for increasing the contrast of SEM images at the certain incident electron energy in which the maximum yield $(\delta_t+\delta_s)$ occurs. As shown in the curves of δ_s for Au and Al targets, these theoretical curves δ_s are closely in agreement with experiments δ of Thomas and Pattinson (1970) for $E_0 \leqslant 1.5$ keV, and for $E_0 > 1.5$ keV the experimental δ become larger than theoretical δ_s because of the dependence on the reduced depth, $y_d=d/R$, of the film thickness d and the penetration range R in equation (24).

8. Lateral distribution of secondary electron emission

The secondary electron yield $\delta(z)$ ejected from the surface at a distance z from the centre of the primary beam can be considered in similar manner. From the geometrical relation to the travelling distance l of secondary electrons given by

$$\propto l=\alpha x/\cos\theta=\alpha R y(1+\tan^2\theta)^{1/2}$$

with $\tan\theta = z/x$, the absorption term of secondaries can be derived as

$$\exp(-\alpha x/\cos\theta)=\exp[-\alpha R(y^2+(z/R)^2)^{1/2}]. \quad (26)$$

Accordingly, the secondary yield $\delta_p(z)$ and $\delta_B(z)$ due to primary and back-scattered electrons, respectively, are given by

$$\delta_p(z)=(K/2)(c_0/\alpha)^{n/(1+n)}\int_0^1\left(\frac{n}{1+n}\right)(1-y)^{-1/(1+n)}A^{n/(1+n)} \times\exp\{-\alpha R[y^2+(z/R)^2]^{1/2}\}\,dy \quad (27)$$

$$\delta_B(z)=(K/2)\eta_B(c_0/\alpha)^{n/(1+n)}\int_0^{1/2}\left(\frac{2n}{1+n}\right)(1-y)^{(n-1)/(n+1)}A^{n/(1+n)} \times\exp\{-\alpha R[y^2+(z/R)^2]^{1/2}\}\,dy. \quad (28)$$

Figures 5(a) and (b) show a comparison of the lateral distribution of secondary electrons $\delta(z)=\delta_p(z)+\delta_B(z)$ for Al and W targets, respectively, of thickness d=50 and 100 Å. These lateral distributions of the secondaries are important to determine the ultimate resolving power of the SEM. The distribution for Al target is broader than the distribution for a W target, in spite of the fact that r for Al is smaller than for W (r=0.2 for Al and 0.43 for W, respectively, calculated from Ono and Kanaya 1979), because the contribution of the back-scattered electrons for thin films may be very small. It is found that the contribution of the escape depth of secondaries is dominant for the sharp lateral distribution, and then we can expect sharp lateral distribution (higher resolution in SEM) when the escape depth of secondaries in the specimen is short. Moreover, it is shown the yield of $\delta(z)$ for Al target in the thickness d=50 Å have a maximum yield at about 20 keV, relating with the film thickness and the escape depth of secondary electrons (x_α=38 Å for Al).

9. Conclusions

(1) Based on the exponential power law for the screened atomic potential, secondary electron emission due to both primary and back-scattered electrons penetrating into metallic elements and semi-conducting compounds is developed in terms of the ionisation loss in the first collision for the escaping electrons.

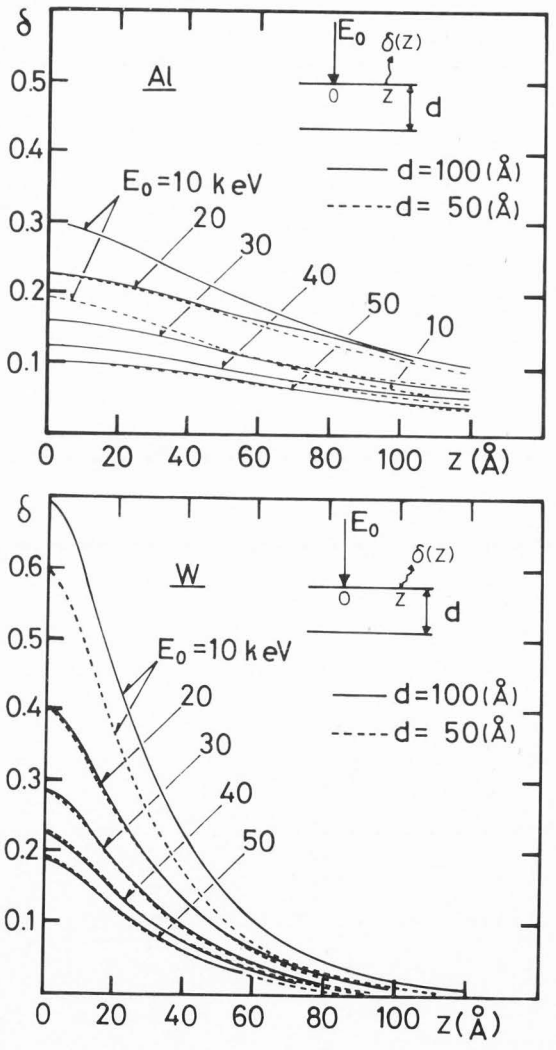

Figure 5. (a) The lateral distributions of electrons for (a) Al and (b) W targets for thickness d=(——) 100 and (---) 50 Å.

(2) The maximum yield and the corresponding primary energy can both consistently be derived as functions of three parameters: atomic number, first ionisation energy and back-scattering coefficient.
(3) The yield-energy curve as a function of the incident energy and the back-scattering coefficient are in good agreement with the experimental results.
(4) The energy dependence of the yield for thin films and the lateral distribution of secondary yield are derived as functions of the back-scattering coefficient and the primary energy.

Ⅲ Secondary Electron Emission from Insulators

1. Introduction

In recent years much interest has arisen in the use of secondary electron emission from bombardment of various solid targets with a finely focused and highly accelerated beam of electrons for scanning electron microscopes. Accordingly, the quantitative analysis of secondary electron microscope images requires a knowledge of the yield and depth in the different energy ranges. The phenomenon of secondary electron emission from solids was discovered by Austin and Starke in 1902 and has since been the subject of numerous experimental and theoretical investigators.

The elementary theory of secondary emission developed by Salow (1940), Baroody (1950), Bruining (1954) and the surveys by McKay (1948), Kollath (1956), Dekker (1958) and Hachenberg and Brauer (1959) have been generalised and modified to incorporate recent range measurements, by Glendenin (1948), Katz and Penfold (1952), Young (1956), Holliday and Sternglass (1959) and Cosslett and Thomas (1964a,b). Results based on the empirical approach were obtained, in paticular, in the work of Kanaya and Kawakatsu (1972), using the Lindhard power potential depending on the incident energy. Similar models by Thomas and Pattinson (1970), Lye and Dekker (1957), Jonker (1954a, b), Dionne (1975) were presented which were in agreement with the experimental work. However, the models cannot explain the very high yield of insulators (BaO 8, KCl 13, NaCl 16) and large escape distance (oxides 50-200 Å, alkali halides 100-500 Å) especially different values of the yield reported for the same compound (e.g. NaCl 6.5, 11 and 16). These values seem to be related to the plasmon losses which occur in integral multiples of a first, lower value, indicating that the same inelastic event was repeated in multiples.

An attempt (Kanaya, Ono and Ishigaki 1978) has been made to present a sufficient solution of the high yield of insulators and to explain the different yields appearing integral multiples, combining the free-electron scattering theory with the plasmon theory.

By using the potential function of the power and exponential forms as a function of a modified screened atomic radius for scattering (Kanaya and Ono 1976), the range-energy relationship of $R=(E_0/E_R)^{1+1/n}/C$ in the energy between 1 keV and 1 MeV is used as the fundamental equation, where n indicates the degree of screening (n goes from 1 to ∞ as the accelerating voltage decreases).

The purely classical empirical theory (Bruining 1954, Jonker 1952, 1954a, b, Lye and Dekker 1957, Kanaya and Kawakatsu 1972) is developed by the power law concerning the energy loss. Also, on the assumption that the absorption is of the Lenard type and that the distribution of secondary electrons generated by both incident and back-scattered electrons within the target is isotropic, the universal yield-energy curves are deduced. It can be shown that the average energy generated by the first collision of incident electrons is E_s=100-200 eV (Rauth and Simpson 1964) and that the secondary escaping beam returns back to the surface suffering a plasmon loss ΔE=10-50 eV, because of the large energy gap of insulators (10 eV).

Since the resulting maximum yield δ_m depends mainly on the energy-range coefficient C of the primary beam and the absorption coefficient α, it can be given as a function of ionisation potential I, valence electron ν (or plasmon loss ΔE) and back-scattering coefficient r as well as the free-electron density $NZ=N_a(\rho/A)Z$ where N_a is the Avogadro's number, ρ the density and A the atomic weight.

2. Absorption coefficient α and escape depth x_α

The high yield δ=1.5-20 of secondary electron emission from insulators due to electron bombardment may be caused by the very large escape depth x_α=500-1000 Å; namely the small absorption coefficient. Then, the most dominant energy losses are considered to the suitably averaged ionisation loss in the first collision and to the plasmon loss due to the interaction with the valence electrons for the escaping secondaries because of the large energy gap about 5-15 eV.

Suppose that the secondary electrons are distributed according to the Lenard (1918) law after release, and satisfy the special case n=4 of the power law in the first collision.

Since their experimental energy E_s=100-200eV is very low compared with the incident $E_0 \geqslant 5$ keV, the transmission fraction of secondaries is given by

$$i_s/i_{s0}=\exp(-N_p\sigma_p x)=\exp(-\alpha x) \qquad (1)$$

where $N_p=N_a\rho\nu/A$ is the electron density contributing the plasmon loss, ν the number of valence electrons per unit volume and σ_p the scattering cross-section due to plasmon loss.

The amount of energy transfer can only occur in integral multiples of the elementary energy loss of $\hbar\omega_p$ (Marton et al 1954), where ω_p is the frequency of plasma oscillations ($\hbar=h/2\pi$), and the total cross-section $N_p\sigma_p$ (Ferrell 1956) becomes

$$N_p\sigma_p=\lambda_p^2(\theta_E/a_H)\ln(4E/\Delta E) \qquad (2)$$

in which

$$\theta_E=\Delta E/2E, \quad \Delta E=28{\cdot}8(\rho\nu/A)^{1/2}\,(\mathrm{eV})$$

and $$N_p=\Delta E^2/(16\pi a_H^3 E_R^2)$$

where λ_p^2 is the correction factor necessary at low energy, E≲1 keV.

Accordingly, the most probable escape depth of secondaries x_α is from $i_S/i_{S0} = 1/e$ and $E=E_S$, given by

$$x_\alpha = \frac{1}{\alpha} = \frac{2a_H E_s}{\lambda_p^2 p \Delta E \ln(4E_s/\Delta E)} \qquad (3)$$

where p is the normalised ratio of one plasmon loss ΔE_p under consideration to the most probable plasmon loss ΔE; $p=\Delta E_p/\Delta E$.

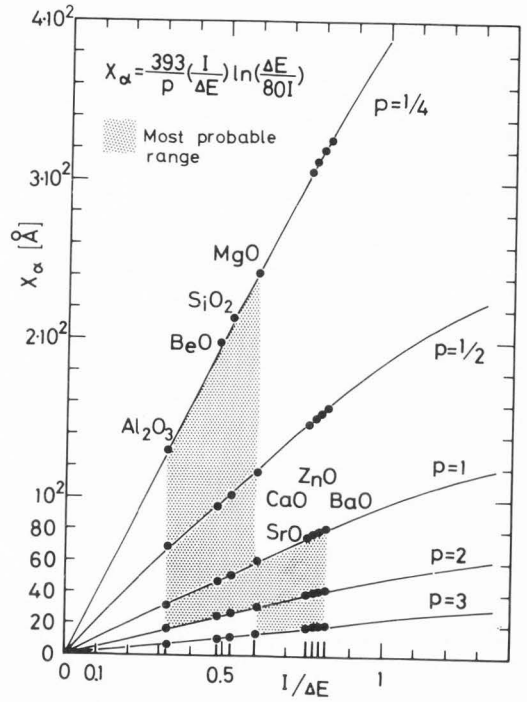

Figure 1. Escape depth x_α of secondary electron emission for insulators of metallic oxides. (Dotted area shows the range between maxima and minima of the experimental results.)

Owing to the ionisation E_S varies between 153 and 232 eV for Al_2O_3 (Rauth and Simpson 1964), and it can be approximated as

$$E_S = n_S I$$

where I is the first ionisation energy and n_S=20 from the assumption of E_S=190 eV and I=9.46 eV for Al_2O_3.

Accordingly, based on the empirical approach, the most probable escape depth of secondary electron emission x_α can be obtained:

$$x_\alpha = \frac{393}{p}\left(\frac{I}{\Delta E}\right)\ln\left(\frac{\Delta E}{80I}\right) (\text{Å}) \qquad (4)$$

where λ_p^2 =0.054 is used.

Figures 1 and 2 show the calculation results of x_α vs I/ΔE.

After Seiler (1967), the maximum exit depth of secondary electrons is approximately five times larger. Then the maximum range for insulators is approximately given by

$$R = 5x_\alpha \qquad (5)$$

which is much larger than the metallic elements.

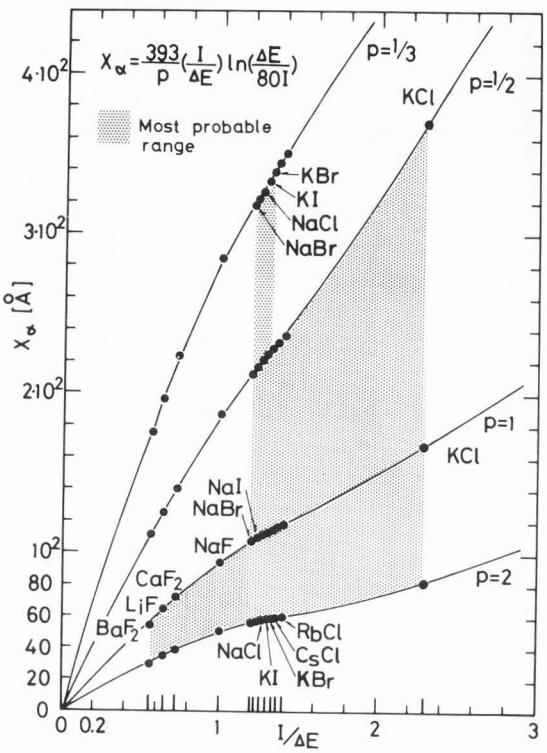

Figure 2. Escape depth of secondary electron emission for insulators of alkali halides x_α as in figure 1. (Dotted area shows the range between maxima and minima of the experimental results.)

3. Universal yield-energy curve

According to the elementary theory and the experimental result (Kanter 1961), the number of secondaries released in the solid is proportional to the energy loss, and these secondaries are isotropically distributed in a solid target, following the absorption law after they are released.

Suppose a primary beam current i_0 falls perpendicularly on a solid target, as shown in figure 3. The secondary emission current i_S originates at a point x and reaches the surface by travelling a distance $\ell = x/\cos\theta$ through the material; it is given as

$$i_s = \left(\frac{K}{2}\right) i_0 \int_0^R \left(\frac{dE/E_R}{dx}\right) \int_0^{\pi/2} \exp(-\alpha x/\cos\theta) \sin\theta \, d\theta \, dx \qquad (6)$$

where K is the constant depending on the penetration of electrons. By using the range-energy relationship I(8) and the resulting energy retardation formula I(9), the secondary yield due to primary electrons $\delta_p = i_S/i_0$ can be given by

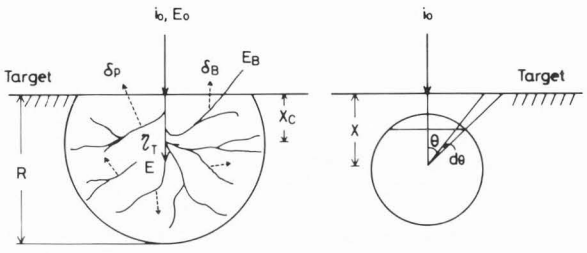

Figure 3. Production of secondary electron emission.

$$\delta_p=\left(\frac{K}{2}\right)\left(\frac{C}{\alpha}\right)^{n/(1+n)}\int_0^1\frac{n}{1+n}A^{n/(1+n)}(1-y)^{-1/(1+n)}$$

$$[\exp(-Ay)+Ay\,E_i(-Ay)]\,dy \qquad (7)$$

Where $A=\alpha R=(\alpha/C)(E_0/E_R)^{1+1/n}$ and $E_i(-x)=-\int_x^\infty[\exp(-t)/t]dt$ is the function of the exponential integral.

Most incident electrons are scattered through small angles as they interact with atoms. As the penetration increases, the primary beam spreads in a Gaussian manner, as shown in the previous paper of diffusion model (Kanaya and Ono 1978). Consideration of these back-scattered electrons becomes especially important because their energy maxima are ranged between 500 and 2000 eV.

According to Kanter (1961), the back-scattered electrons that diffuse back from the interior of the material follow a cosine distribution. Therefore the rates of energy dissipated are large compared with those of the incoming primaries. Thus the secondary electron yield cannot be disregarded when the back-scattering coefficient η_B is relatively large.

Consider the production of secondary electrons by back-scattered electrons, from the generalised case of primary electrons. The secondary yield δ_B is given by

$$\delta_B=\eta_B\left(\frac{K}{2}\right)\left(\frac{C}{\alpha}\right)^{n/(1+n)}\int_0^{1/2}\left(\frac{2n}{1+n}\right)(1-y)^{(n-1)/(n+1)}A^{n/(1+n)}[\exp(-Ay)$$

$$+Ay\,E_i(-Ay)]\,dy \qquad (8)$$

where η_B is the back-scattering coefficient.

The total secondary yield is then considered to be the sum of the primary and back-scattered electrons:

$$\delta=\delta_p+\delta_B. \qquad (9)$$

It can be simply given by

$$\delta/(K/2)(C/\alpha)^{n/(1+n)}=f_p(A)+\eta_B f_B(A) \qquad (10)$$

in which $f_p(A)$ and $f_B(A)$ are the integrations in (7) and (8), respectively and have maxima as shown in figure 4.

Accordingly, the value of total yield normalised by the maximum yield, δ/δ_m, can be obtained as a function of E/E_m.

$$\delta/\delta_m=[f_p(A)+\eta_B f_B(A)]/[f_p(A)+\eta_B f_B(A)]_{max} \qquad (11)$$

for $E/E_m=(A/A)^{n/(1+n)}$.

For the sake of simplicity for the calculation, it can be numerically approximated as

$$[f_p(A)+\eta_B f_B(A)]_{max}=0{\cdot}365\,(1+1{\cdot}26\,r)$$

and

$$A_m=(1+5\,r^2) \qquad (12)$$

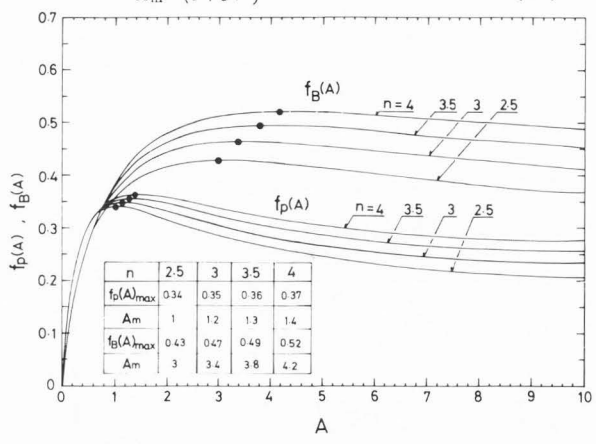

Figure 4. The variation of secondary yield normalised by the maximum yield, δ/δ_m, can be obtained as a function of E/E_m.

where the back-scattering coefficient $r=|\eta_B|_{x/R=\frac{1}{2}}$ is used. Figure 5 represents the universal yield-energy curve as a function of the energy dependent parameter n, where the upper limit of the curve among the most probable range corresponds to the alkali halide $I/p\Delta E=4$ and the lower limit to the metallic oxide $I/p\Delta E=0.5$, respectively, and the yield increases as the ratio of $I/p\Delta E$ increases.

The energy and back-scattering dependence of the universal yield-energy curves as shown in figure 6 are in good accordance with experimental results, where the values in round brackets are used as experimental points.

4. Quantitative characteristics of secondary electron emission

The value of the incident energy for which the maximum yield occurs is related to α and C as follows:

$$(E_m/E_R)^{1+1/n}=(C/\alpha)A_m=(C/\alpha)(1+5r^2).$$

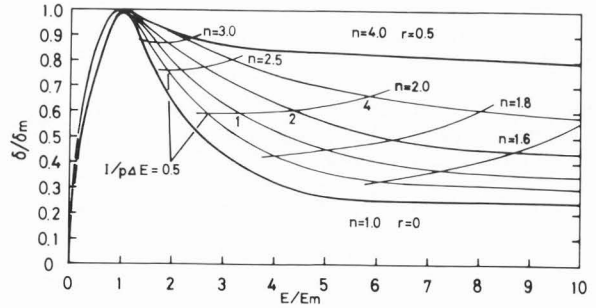

Figure 5. Universal yield-energy curve as a function of n and $I/p\Delta E$.

Target	Ref.		δm (Exp.)	Em (Exp.) [eV]
□ KCl	Ardenne	(1962)	7.1~12.4 (8.1)	713 ~ 1200 (1200)
● KBr	Petzel	(1958)	14. (12.5)	1400 (1500)
△ MgO	Dekker	(1958)	14. (16 ~ 24)	1200 (1200)
▲ Al_2O_3	Dawson	(1966)	5.4 (4.7)	610 (600)
○ MgO	Johnson & Mc Kay	(1954)	4.5~ 7.8 (7.1)	525~ 910 (~ 1000)
× BeO	Bronshtein et al	(1968)	3.47(3 ~ 5)	412 (450)

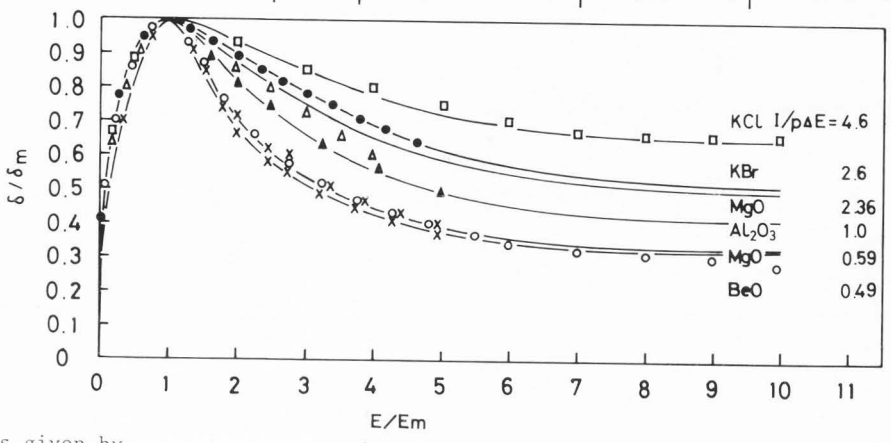

Figure 6. The theoretical and experimental comparison of the yield-energy curve.

Then, from I(8) and (3), it is given by

$$(E_m/E_R)^{1+1/n}=\frac{(E_s/E_R)}{\lambda_p^2 p\ln(4E_s/\Delta E)}\frac{\pi(n+1)}{(n-1)}\Gamma^2\left(\frac{1}{n}\right)\sin^2\left(\frac{\pi}{2n}\right)a^2\left(\frac{a_H}{a}\right)^{2/n}\times\left(\frac{NZ^2}{\pi a_H \nu}\right)^{1/2}(1+5r^2). \quad (13)$$

For the assumption n=4 in the first collision, which corresponds to the energy E_m=0.5-2 keV, and the empirical data for NaCl; E_m=690 eV, I=10 eV, ΔE =7.85 eV, ν=2, it follows that

$$E_s/\lambda_p^2\ln(4E_s/\Delta E)=629\ (\mathrm{eV}).$$

Accordingly, the characteristic energy E_m is simply approximated as

$$E_m=58{\cdot}3\left(\frac{I(1+5r^2)}{p}\right)^{0{\cdot}8}\left(\frac{\rho}{A\nu}\right)^{0{\cdot}4}Z^{0{\cdot}6}\ (\mathrm{eV}) \quad (14)$$

where E_S=200 eV, n_S=20, and λ_p^2=0.054 are determined empirically.

On the other hand, the maximum yield δ_m is given by

$$\delta_m=\frac{K}{2}\left(\frac{C}{\alpha}\right)^{n/(1+n)}0{\cdot}365(1+1{\cdot}26\,r).$$

According to the empirical relationship δ_m/E_m leads to

$$\frac{\delta_m}{E_m}=\left(\frac{K}{2}\right)\frac{0{\cdot}365\,(1+1{\cdot}26\,r)}{E_R(1+5\,r^2)^{4/5}}\simeq C_0(1+1{\cdot}26\,r)$$

where $C_0=7.4\times10^{-3}\mathrm{eV}^{-1}$ is the best fit to δ_m=0.65 for NaCl. Then the maximum yield δ_m for insulators is empirically given by

$$\delta_m=0{\cdot}43(1+1{\cdot}26\,r)\left(\frac{I(1+5\,r^2)}{p}\right)^{0{\cdot}8}\left(\frac{\rho}{A\nu}\right)^{0{\cdot}4}Z^{0{\cdot}6}. \quad (15)$$

The back-scattering coefficient r is given by the diffusion model (Kanaya and Okayama 1972, Kanaya and Ono 1978).

$$r=\tfrac{1}{2}(1-\cos\theta_0) \quad (16)$$

with $\tan\theta_0=2.2\gamma(1+\gamma)/(1+2\gamma-0.21\gamma^2)$ in which γ is the constant in the transmission fraction of the beam such as $\eta_T=\exp(-\gamma y/1-y)$.

The energy dependence of γ is given by combining the diffusion effect due to multiple collisions and the energy retardation in accordance with a modified Thomson-Whiddington law (Kanaya and Ono 1978)

$$\gamma=\Omega(n-1)(Z+1)/[n(n+1)2^{1/n}] \quad (17)$$

with

$$\Omega=\frac{1}{3}\left(\int_0^{\pi/2}d\Omega+\frac{1}{2!}\int_{\pi/2}^{3\pi/4}d\Omega+\frac{1}{3!}\int_{\pi/2}^{5\pi/6}d\Omega\right)$$

$$d\Omega=\sin\theta\,d\theta/(1+\cos\theta)^{1+1/n}.$$

In the present calculation, r used is near the maximum value corresponding to E_0=500-2000 eV for Z from 1 to 100 which is very close to the experimental result by Weinryb and Philibert(1964).

Figures 7 and 8 show the maximum yield values for insulators of metallic oxides and alkali halides corresponding to their characteristic energies which are shown in figures 9 and 10. The experimental results are from Bruining and De Boer (1939a,b), Hachenberg and Brauer(1959), Knoll et al(1944), and

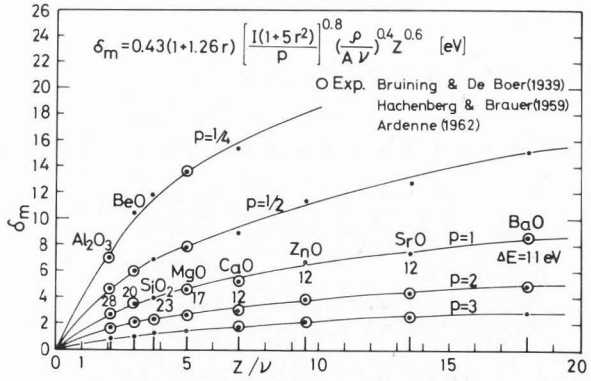

Figure 7. Maximum secondary electron emission yield for insulators of metallic oxides.

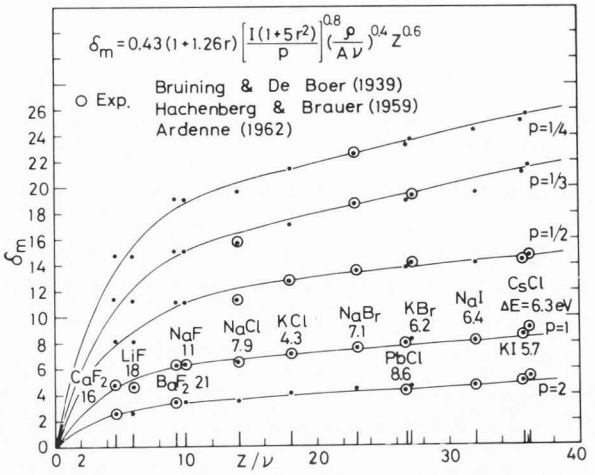

Figure 8. Maximum secondary electron emission yield for insulators of alkali halides.

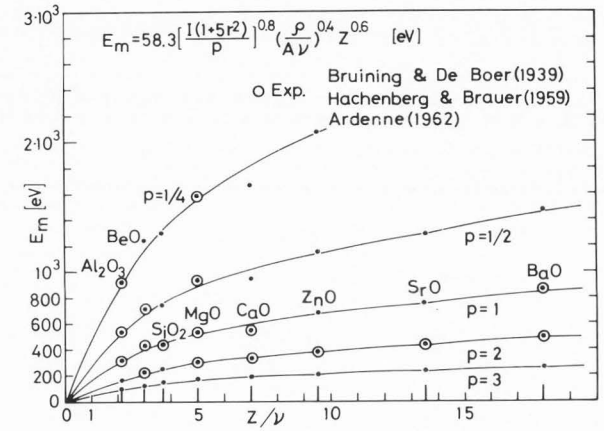

Figure 9. Characteristic energy of secondary electron emission given maximum yield for insulators of metallic oxides.

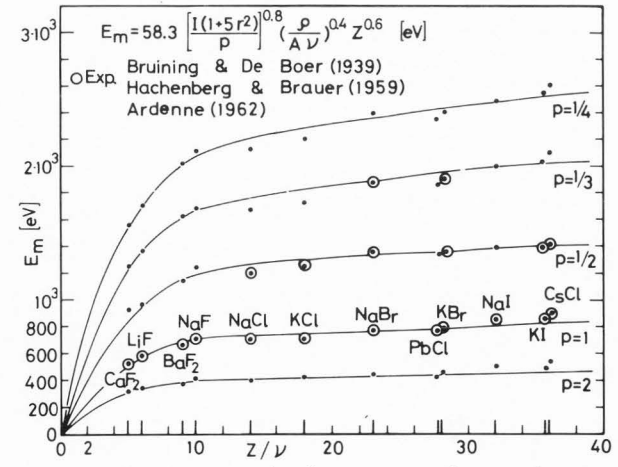

Figure 10. Characteristic energy of secondary electron emission given maximum yield for insulators of alkali halides.

Table 1. Secondary emission characteristics calculated.

Insulators	Z	ρ (g cm^{-3})	A (g)	ν	ΔE (eV)	I (eV)	r	E_m (eV)	δ_m	$\frac{\delta_m}{C_0 E_m}$	x_t (Å)
Al_2O_3	50	3·90	102	24	27·60	9·46	0·17	350	3·10	1·21	31
BeO	12	3·02	25	4	20·00	9·8	0·113	412	3·47	1·14	47
SiO_2	30	2·30	60	8	15·90	11·8	0·18	429	3·90	1·23	50
MgO	20	3·65	40	4	17·40	10·3	0·12	525	4·50	1·15	60
CaO	28	2·62	56	4	12·40	9·9	0·22	537	5·10	1·28	77
ZnO	38	5·60	81	4	12·30*	10·0	0·25	677	6·65	1·32	80
SrO	46	4·70	104	4	12·23	9·6	0·26	742	7·30	1·33	75
BaO	72	5·72	153	4	11·13	9·4	0·28	850	8·50	1·35	81
CaF_2	38	3·18	78	8	16·45	12·0	0·20	522	4·82	1·25	70
LiF	12	2·29	26	2	17·80	11·9	0·11	561	4·73	1·14	66
BaF_2	74	4·82	175	8	20·70	11·0	0·24	665	6·35	1·3	56
NaF	20	2·79	42	2	10·50	11·3	0·18	698	6·36	1·23	96
NaCl	28	2·16	58	2	7·85	10·0	0·22	690	6·50	1·28	108
KCl	36	1·98	74	2	4·33	10·0	0·27	713	7·10	1·34	175
NaBr	46	3·20	103	2	7·10	8·5	0·28	782	7·80	1·35	104
RbCl	54	2·76	120	2	6·17	8·6	0·27	765	7·60	1·34	116
KBr	54	2·75	119	2	6·19	8·1	0·31	779	8·00	1·39	111
NaI	64	3·66	150	2	6·36	8·0	0·30	775	8·10	1·38	107
KI	72	3·12	160	2	5·68	7·4	0·34	844	8·87	1·42	110
CsCl	72	3·97	168	2	6·26	8·4	0·32	877	9·10	1·40	113

Physical data refer to Frederikse (1963). ΔE is the most probable value for p=1, where 12.3* for ZnO is used to the reduced value.
$C_0 = 7.4\times10^{-3}$ eV^{-1}.

Ardenne (1962). Also, the physical characteristics of insulators necessary for the calculation are shown in table 1, where all data are considered to be the mean values of compounds, and for Al_2O_3, SiO_2, CaF_2 and BaF_2 valence electrons are considered to be the sum of the innermost and outermost shells, and for all others are assumed to be for the outermost shell.

The highest yield values of insulators which are experimentally obtained by single crystals such as NaCl(16), KCl(12), NaBr(19 and 23), KBr(13 and 19) due to the lower plasmon losses $p=\frac{1}{2}\sim\frac{1}{4}$, since the lattice band is very tight, can be quantitatively evaluated by the plasmon theory.

5. Conclusions

(1) Based on the power and exponential potential law, the secondary electron emission due to primary and back-scattered electrons penetrating in insulators is derived, combining the ionisation loss in the first collision with the plasmon loss for the escaping secondary emission.
(2) The yield-energy curve as a function of the incident energy and the back-scattering coefficient are in good agreement with the experimental results.
(3) The maximum yield at the characteristic energy can both consistently be related with the three parameters: ionisation potential, valence electrons and back-scattering coefficient.
(4) The high yield of insulators and large escape distance and especially different values of the yield in the same compound are explained by the different plasmon losses occurring in any multiple that lower plasmon loss was repeated in multiples.

IV Energy Dependence of Secondary Electron Emission, Resolving Power and Temperature-Rise of Specimens

1. Introduction

Secondary electrons are ejected from the surface of an object by the electron beam which is focused to a very small spot and is scanned over the specimens. From these electrons, which are collected and amplified, an integrated picture of varying intensities can be obtained and observed on the cathode-ray tube which corresponds to the scanning point on the specimen. To obtain high resolution it is important to use specimen yielding high secondary electrons and to optimize operating conditions which will minimize thermal damage.

Over the past several decades many authors have analytically calculated the secondary electron yields based on the elementary theory of secondary emission mechanisms. Reimer(1968), Shimizu and Murata(1971) and Shimizu(1974) have recently estimated the secondary yields by Monte Carlo techniques.

The analytical treatments as well as Monte Carlo calculations are very useful to evaluate the secondary electron emission mechanisms by an electron beam impact. Since the Bethe's energy loss formula may be not enough to give the good satisfaction with the experimental results related to the penetration range of the incident electrons, the second approximation formula (Spencer 1954,55,59, Berger & Seltzer 1964) for the energy loss has been used for the Monte Carlo calculation by Shimizu (1974). In our analytical treatments (Ono and Kanaya 1974b), the secondary yields are calculated as a function of the accelerating voltage, by using the energy loss formula based on the power potential in which the penetration range is in good agreement with the experiments over the energy range hundreds eV to several MeV (Young 1956, Holliday and Sternglass 1959, Glendenin 1948, Cosslett and Thomas 1964a, 1964b, 1965, Seliger 1955, Wright and Trump 1962, Lonergan et al 1970 and Rester and Derrickson 1971).

One of the purposes of the present work developed from the theory of Ono et al.(1974a, b) is to calculate the image contrast and the resolving power in the scanning electron microscope, based on the theory of Simon (1969) and Everhart et al. (1959, 1972), by evaluating the secondary electron emission yield as a function of the accelerating voltage. The other purpose is to estimate the temperature-rise of the specimen and determine operating conditions to reduce the thermal damage in a scanning electron microscope (Ono et al 1977).

2. Energy dependence of secondary electron emission due to primary and back-scattered electrons

Secondary electrons are emitted from a solid surface when primary electrons bombard the target. The secondary yield, δ, which is defined as the ratio of the number of electrons emitted by the electron beam bombardment to the incident number of electrons, varies directly in inelastic collisions. According to elementary theory by many authors the secondary electrons ejected from the target increase in proportion to the energy loss and are isotropically distributed in the Lenard law after being dislodged.

The analytical treatment, as well as Monte Carlo calculations, are very useful to evaluate the secondary electron emission mechanisms from metals by electron beam bombardments, which have been developed by Dekker (1958), Jonker (1952) and others, Reimer (1968), Shimizu (1971, 1974) and Koshikawa and Shimizu (1973), respectively.

In this analytical treatment, the secondary yield, in which the constant K involving the surface condition of the specimen is empirically decided from most of Shimizu's data of secondary yield, is calculated as a function of the accelerating voltage by using the energy loss formula derived from the power potential. The results are in close agreement with both experimental and Monte Carlo calculation of Shimizu (1974) using a modified Bethe's energy loss formula by Spencer and Fano (1954). Consider an incident electron beam which falls perpendicularly on a solid target. The number of secondary electrons released is proportional to the electron energy loss dE/dx. They arrive at the surface by travelling a distance $\ell=x/\cos\theta$, after exponential absorption by the target, and are emitted from the target surface depending on the surface transmission coefficient (Sternglass 1950, 1957, and Kanaya and Ono 1974) and the mean energy of secondaries $\bar{E}_B$. The secondary electron yield δ_p due to the primary electron is given by

$$\delta_p = \left(\frac{K}{2}\right)\int_0^R\int_0^{\pi/2}\left(\frac{dE}{dx}\right)\exp\left(-\frac{\alpha x}{\cos\theta}\right)\sin\theta d\theta dx, \qquad (1)$$

where K is a constant which is determined empirically and α the absorption coefficient.

Assuming that the fractional distribution of secondary electrons in a solid is simply expressed as $i_s/i_p=\exp(-\alpha x)=1/e$, the absorption coefficient α can be determined by the absorption mean length of x_α as

$$x_\alpha=1/\alpha=2.67A_0 I/\rho Z^{2/3} \quad [\text{Å}] \qquad (2)$$

where i_s is the secondary emission current, i_p the primary electron current.

By using the range-energy relationship of $R=E_0^{1+1/n}/c_0$ and resulting energy relationship formula of

$$E/E_0=(1-y)^{\frac{n}{1+n}} \qquad (3)$$

where $y=x/R$ is the reduced range, the rate of energy loss is then given by

$$\frac{dE}{dy}=-\frac{n}{1+n}(Rc_0)^{\frac{n}{1+n}}(1-y)^{-\frac{1}{1+n}} . \qquad (4)$$

By substituting eq.(4) with eq.(3) into eq.(1), the secondary yield δ_p becomes

$$\delta_p = \left(\frac{K}{2}\right)\left(\frac{n}{1+n}\right)E_0\int_0^1\int_0^1 (1-y)^{-\frac{1}{1+n}}\exp\left(-\frac{By}{z}\right)dzdy \quad (5)$$

where $z=\cos\theta$ and $B=\alpha R$. By introducing the new variable $r=(1-y)^{n/(1+n)}$, the secondary yield δ_p is expressed as

$$\delta_p = \left(\frac{K}{2}\right)E_0\int_0^1\int_0^1 \exp\left\{-\frac{B}{z}\left(1-r^{1+\frac{1}{n}}\right)\right\}dzdr. \quad (6)$$

The secondary yield δ_B due to the back-scattered electrons can also be expressed as

$$\delta_B = \eta\left(\frac{K}{2}\right)E_0\int_{\bar{k}}^1 \bar{k}^{1+\frac{1}{n}}\int_0^1 \exp\left\{-\frac{B}{z}\left(t^{1+\frac{1}{n}}-\bar{k}^{1+\frac{1}{n}}\right)\right\}dzdt \quad (7)$$

where η is the back-scattering coefficient and $\bar{k}$ the relative energy of back-scattered as given by Sternglass (1957),

$$\bar{k} = 0.45+2\cdot 10^{-3}Z$$

for $E_0 = 0.2\sim3.2$ keV where Z is the atomic number. Also, the energy spectrum of back-scattered electrons has been confirmed by the experiments (Kulenkampff and Spyra 1954, and Darlington 1975). Then, the secondary electron emission yield δ_B can be calculated by using the back-scattered coefficient which can be empirically formulated as a function of the incident energy as shown in figure 1, comparing with the experimental and Monte Carlo calculation by Bishop(1965,66), Wittry (1966, 1967, 1970), Shimizu and Murata (1971) and Shimizu(1974). More detailed calculations of η based on a diffusion model have been shown in Section I-fig.14.

Figures 2 and 3 show the yield δ_p and δ_B, and the total yield δ_t of Au, W, Al and C as a function of the incident energy E_0, respectively.

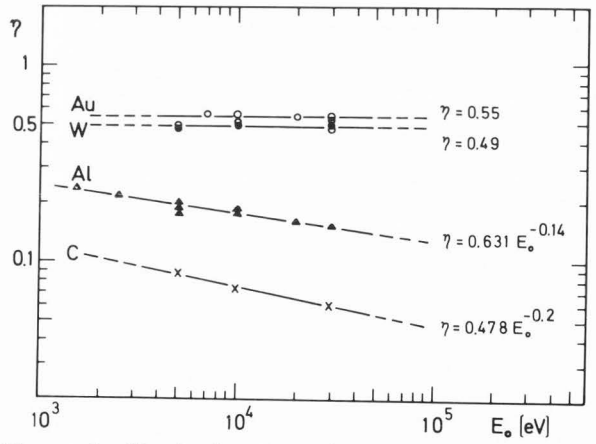

Figure 1. The back-scattering coefficient η versus the incident energy E_0. [○ Au, ● W, ▲ Al, × C; Wittry (1966, 1967, 1970). Full lines illustrate by empirical formulations for the incident energy.]

The theoretical results based on the power and exponential potential are compared with the experimental results by Kanter(1961), Kollath(1956) and Wittry(1966) and Monte Carlo calculation by Shimizu(1974); however, the yields in Au and W seem to be large because of the assumption of the constant value, η.

3. Energy dependence of resolving power and contrast

Since the signal of secondary electrons collected and amplified by the multiplier when a finely-focused beam bombards a point in the specimen suface is used to control the brightness on a cathode-ray tube and the time during which secondary electrons leave the specimen is very short compared with the time taken to move the focused beam from one point to the next on the specimen, then that time can be neglected in the following calculation.

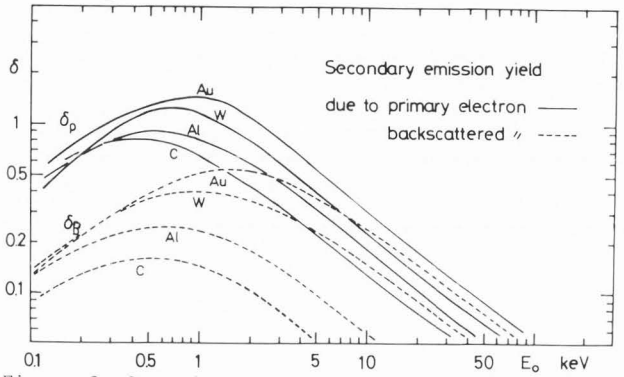

Figure 2. Secondary electron yields, δ_p and δ_B, for the selected materials as a function of the incident energy. The constant K of the materials is used as 0.01 for Au, 0.014 W, 0.021 Al, and 0.016 C.

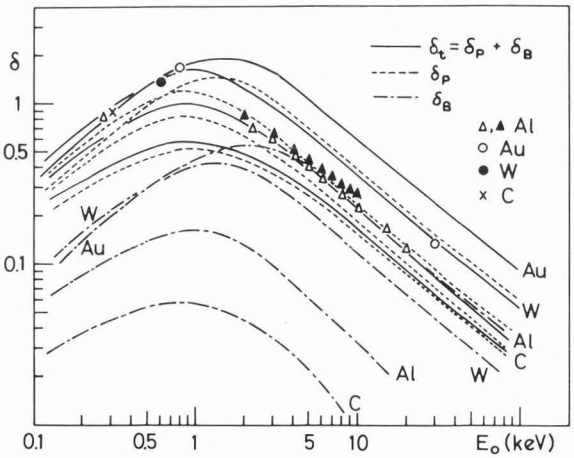

Figure 3. The total secondary electron yield δ_t as a function of the incident energy E_0. Experimental points and Monte Carlo calculations; ○ Au, ● W, △, ▲ Al, and × C by Shimizu (1974), Kanter (1961), Kollath (1956) and Wittry (1966).

The number of secondary electrons N emitted from the specimen surface by the number of primary electrons n striking each picture element on the specimen surface is simply given by $N=\delta n$. If all the secondary electrons emitted from the specimen surface which corresponds to one picture element are collected and amplified by the multiplier, N may be equivalent to the brightness B of that picture element, so that the contrast of image C_0 is written by

$$C_0 = \Delta B/B = \Delta N/N. \tag{8}$$

After Rose (1948), and Shockley and Pierce (1938), the contrast $\Delta B/B$ can be expressed as (Everhart et al 1959)

$$\Delta B/B = S_N\sqrt{(1+1/\delta_t)/n}, \tag{9}$$

where S_N is the signal-to-noise ratio, and $n=I_BT_F/eP^2$. Hence, it follows that

$$\frac{\Delta B}{B} = S_N\sqrt{\frac{eP^2}{I_BT_F}\left(1+\frac{1}{\delta_t}\right)}, \tag{10}$$

where e is the electronic charge, P^2 total picture elements of the cathode-ray tube, I_B the current of the incident beam, and T_F the total recording time per one frame. Figure 4 shows the contrast

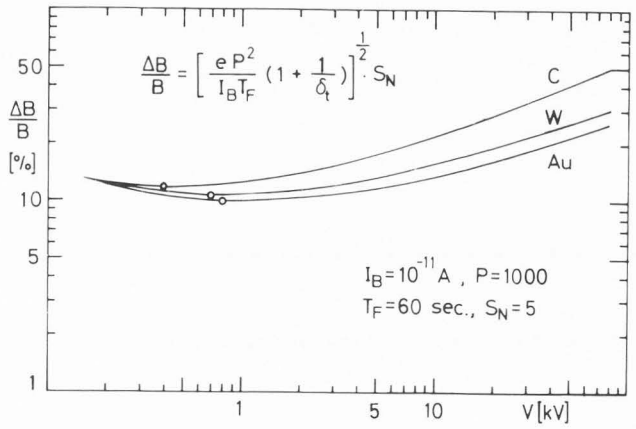

Figure 4. The contrast $\Delta B/B$ as a function of the accelerating voltage V.

$\Delta B/B$ as a function of accelerating voltage under the condition of $I_B=10^{-11}$A, P=1000, T_F=60 sec. and the threshold signal-to-noise ratio S_N=5 for the coated films of C, Au and W.

The incident beam current I_B can be expressed by using eq.(10) as

$$I_B = eP^2(1+1/\delta_t)S_N^2/\{T_F(\Delta B/B)^2\}. \tag{11}$$

Since the above current I_B produces the spot diameter d , it can be obtained from the following well-known relation as

$$I_B = (\pi^2/4)\beta d^2\alpha_0^2, \tag{12}$$

where β is the brightness of the electron beam source and α_0 is the beam aperture on the image side. The minimum beam spot diameter which corresponds to the resolving power d is presented by Simon (1969) and Pease & Nixon (1965), mostly depending on the brightness, spherical- and diffraction aberration as given by

$$d = (8D^3C_S/3\sqrt{3})^{1/4} \tag{13}$$

where $D^2=(4eS_N^2P^2/\pi^2C_0^2T_F)Q+(1.22\lambda)^2$, λ is de Broglie wave length. Then the resolving power d can be written by substituting $Q=1+1/\delta$ and $\beta=J_ceV/(t_{em}\pi B_z)$ into eq.(13) as

$$d = (8C_S/3\sqrt{3})^{1/4}(S_N/C_0)^{3/4}\{4eP^2(1+1/\delta_t)/(\pi^2\beta T_F)\}^{\frac{3}{8}} \tag{14}$$

where C_S is the spherical aberration coefficient, J_c the emission current density on the cathode, V the accelerating voltage, t_{em} the absolute temperature of the cathode, and B_z the Boltzmann constant. Figure 5 shows the resolving power d from eq.(14) as a function of accelerating voltage under the conditions of C_S=1cm, $P^2=10^6$, $S_N/C_0=400$ and T_F=80 sec. for the coating materials of C, Au and W, (data used refer to the results by Broers 1970 and Wells 1974), where $\beta/V=6$(Acm^{-2}strad.$^{-1}V^{-1}$) for tungsten hair-pin cathode, 40 for LaB_6 cathode and 800 for field emission gun, respectively.

4. Temperature-rise of the specimen

Consider the temperature-rise θ_{ta} of the volume when the volume πa^2R is bombarded by the electron beam during the time t_a. The beam with a diameter 2a penetrates into the target to the

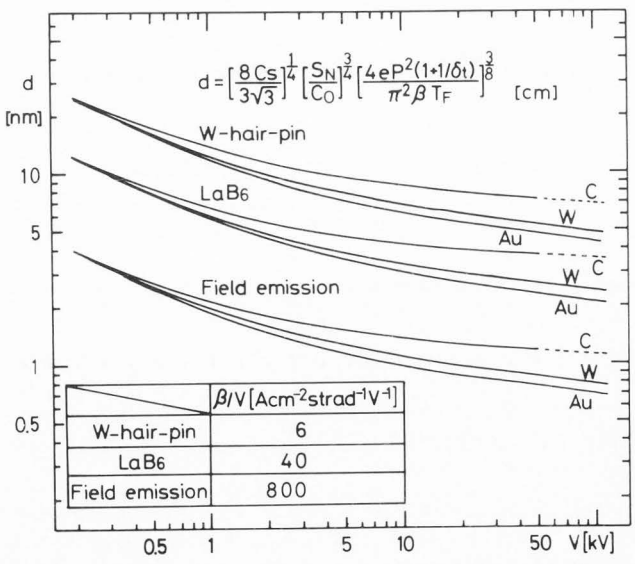

Figure 5. Resolving power d as a function of the accelerating voltage V for various coating materials in SEM.

depth R, and the absorbed heat capacity in the volume $\pi a^2 R$ most effectively influenced by the electron beam bombardment can be expressed from the well-known energy balance relation,

$$I_B E_0 t_a = \pi a^2 R(\theta_{ta} - \theta_0)\rho c 4.186, \quad (15)$$

where I_B is the total current on the specimen, E_0 the accelerating voltage, R the penetration range of the electron, θ_0 the initial temperature of the specimen and ρ and c are the density and the specific heat of the specimen, respectively. Then, the temperature θ_{ta} is obtained under the condition of $\theta_0=0$ as

$$\theta_{ta} = I_B E_0 t_a/(\pi a^2 R\rho c 4.186). \quad (16)$$

On the other hand, the temperature-rise is caused by the energy loss in the volume $\pi a^2 R$ of the target bombarded, and the energy loss is given by eq. I(22) shown in I-Fig.12. The temperature θ_{ta} of the volume when the energy E is absorbed in the volume $\pi a^2 x$ is given by(Ono et al 1974a,b, 77)

$$\theta_{ta} = I_B E t_a/(\pi a^2 x\rho c 4.186). \quad (17)$$

Assuming that the heat generated at a heat pole is conducted in two dimensional directions, the temperature $\theta(t)$ after the time t, which has been reduced by the thermal condition, can be expressed by the solution of the well-known equation

$$\frac{\partial\theta(t)}{\partial t} = \kappa\left(\frac{\partial^2\theta}{\partial x^2} + \frac{\partial^2\theta}{\partial y^2}\right), \quad (18)$$

where κ is the thermal conduction coefficient ($=\lambda_0/c\rho$), λ_0 the thermal conductivity. The solution of eq.(18) from $r^2 = x^2 + y^2$ can be written by

$$\theta(t) = \frac{\pi a^2\theta(0)}{4\pi\kappa t}\exp\left(-\frac{r^2}{4\kappa t}\right), \quad (19)$$

where $\theta(0)$ is the temperature for t=0. Equation (19) differentiated with respect to the time t is written in the normalized form,

$$\frac{d\{\theta(t)/\theta(0)\}}{dt} = \left\{-\frac{a^2}{4\kappa t^2} + \frac{a^2 r^2}{16\pi^2 t^3}\right\}\exp\left(-\frac{r^2}{4\kappa t}\right), \quad (20)$$

By assuming that the characteristic time t_a giving the maximum values can be determined from the condition of

$$\frac{d\{\theta(t)/\theta(0)\}}{dt} = 0, \quad (21)$$

from $-a^2/(4\kappa t^2) + a^2 r^2/(16\kappa^2 t^3) = 0$ and r=a, t_a can be obtained by

$$t_a = a^2/(4\kappa). \quad (22)$$

The mean temperature θ_{ta} of the volume which corresponds to the bombarded area by the beam becomes maximum comparing with the temperature θ_t after a shorter or longer time t than the characteristic time t_a.

Consider the temperature-rise where the object of volume $\pi a^2 x$ is bombarded by the electron beam during the above time t_a. The length of one line R_L scanned on the specimen is

$$R_L = L_{CRT}/M_0, \quad (23)$$

where M_0 is the magnification and L_{CRT} the length of the cathode-ray tube. The scanning line time t_L is

$$t_L = T_F/(2L_n), \quad (24)$$

where T_F is the scanning time per one frame and L_n the number of scanning lines. The mean stored time t_s which is assumed to be stored in the beam size $2a$ when a beam is scanned on the specimen is

$$t_s = t_L/(R_L/2a) = T_F M_0 a/(L_n L_{CRT}). \quad (25)$$

The characteristic temperature θ_{ta}, defined as the temperature-rise when the beam bombarded the volume $\pi a^2 x$ during the time t_a, may be reduced by the thermal conduction after the time t_a. The temperature θ_{ta} of the volume may be reduced to $\theta(2t_a)$ by thermal conduction after the time $2t_a$. The new temperature-rise θ_{ta} may result from the residual energy after $2t_a$ at the same time, because the volume was under continuous beam bombardment. Therefore, the temperature θ_{2ta} of the volume after the time $2t_a$ becomes

$$\theta_{2ta} = \theta(2t_a) + \theta_{ta}. \quad (26)$$

Then, the temperature θ_s of the volume $\pi a^2 x$ after the time t_s can be given by

$$\theta_s = \theta(ft_a) + \theta(f-1)t_a + \cdots\cdots + \theta(2t_a) + \theta_{ta}, \quad (27)$$

where $f=t_s/t_a$, as illustrated in figure 6. Under the condition of the thermal conduction in two dimensions, the temperature $\theta(ft_a)$ is given by

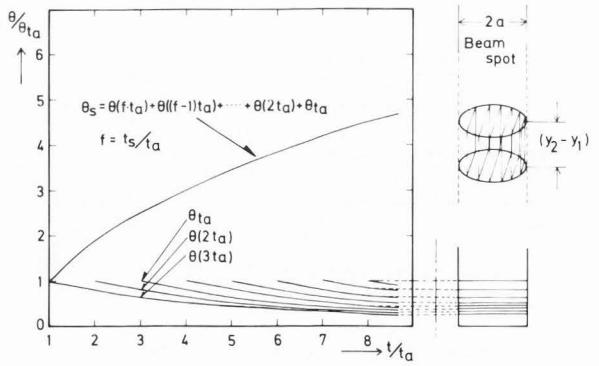

Figure 6. The schematic illustration of the process of the temperature-rise θ_s per volume $\pi a^2 x\ \{=\pi a^2 R(y_2-y_1)\}$ after the time t_s.

$$\theta(ft_a) = \frac{\pi a^2 \theta_{ta}}{4\pi\kappa f t_a} \exp(-\frac{r^2}{4\kappa f t_a}). \qquad (28)$$

Therefore, the temperature θ_s after the time t_s can be obtained by the summation of $\theta(ft_a)$ from f=1 to $f=t_s/t_a=F$,

$$\theta_s = \sum_{f=1}^{F} \frac{\pi a^2 \theta_{ta}}{4\pi\kappa f t_a} \exp(-\frac{r^2}{4\kappa f t_a}). \qquad (29)$$

The temperature θ_s can be written in the form of the integral because t_a is very short compared with t_s practically,

$$\theta_s = \int_0^{t_s} \frac{\pi a^2}{4\pi\kappa t} \exp(-\frac{r^2}{4\kappa t}) d\theta_t$$

$$= \frac{I_B E}{4\pi x \lambda_0 4.186} \int_0^{t_s} \frac{1}{t} \exp(-\frac{r^2}{4\kappa t}) dt \ , \qquad (30)$$

where $d\theta_t = \{I_B E/(\pi a^2 x \rho c 4.186)\}dt$. Let $r^2/4\kappa$ be ξ, $\xi/t=\psi$ and $\xi/t_s=\psi_s$, eq. (30) becomes the exponential integral form as

$$\theta_s = \frac{I_B E}{4\pi x \lambda_0 4.186} \int_{\psi_s}^{\infty} \frac{1}{\psi} \exp(-\psi) d\psi \ . \qquad (31)$$

Hence, the temperature-rise θ_s is given by a simple logarithmic form as

$$\theta_s = \frac{I_B E}{4\pi x \lambda_0 4.186} \{-\ln(\psi_s) - \gamma_0 + \psi_s \cdots\cdots\}, \qquad (32)$$

where $\gamma_0=0.57721$, $\psi_s=r^2/(4\kappa t_s)$. Figure 7 shows the temperature-rise of the volume $\pi a^2 x$ in the specimens (Au, W and C) during the time t_s as a function of the absorbed energy E(x) for a=50 Å, $I_B=10^{-11}$A, where E(x) expressed the absorbed energy integrated as follows

$$E(x) = \int_{x_E^-(x/2)}^{x_E^+(x/2)} E_0 \frac{d(E_A/E_0)}{dx} dx.$$

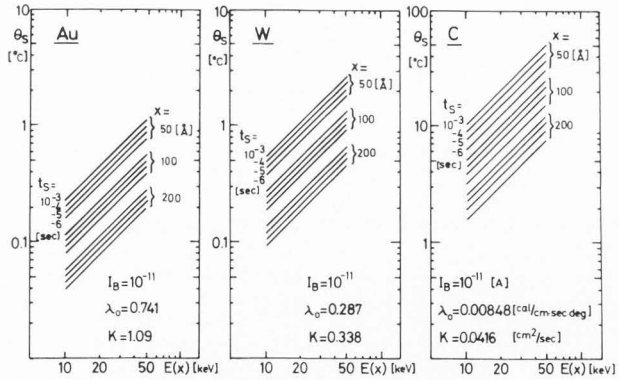

Figure 7. The temperature-rise θ_s of the volume $\pi a^2 x$ in the specimen (Au, W and C) during the time t_s as a function of the absorbed energy E(x) integrated.

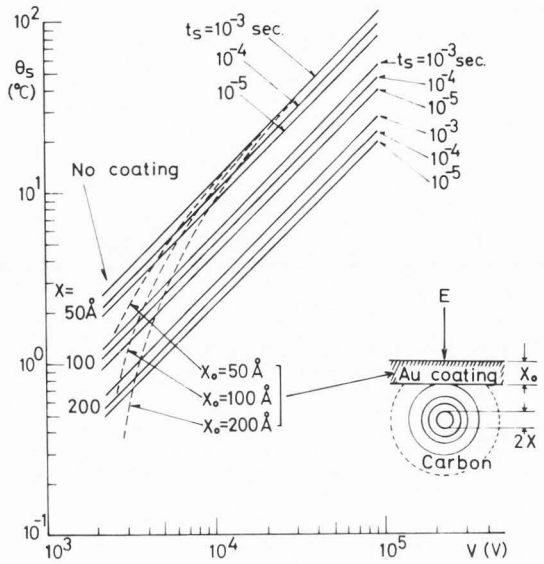

Figure 8. The temperature-rise θ_s of a carbon specimen of volume $\pi a^2 x$ in case of coated with Au and no-coating during the time t_s as a function of the accelerating voltage V; $\lambda_0=0.00848$ [cal $cm^{-1}sec^{-1}deg^{-1}$], $\kappa=0.0416$ [cm^2sec^{-1}], a=50[Å] and $I_B=10^{-11}$[Å].

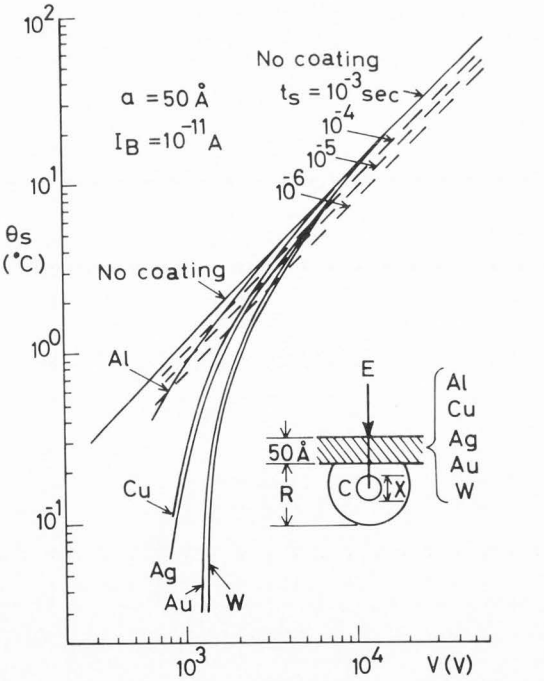

Figure 9. The temperature-rise θ_s of a carbon specimen of volume $\pi a^2 x$ in case of coated with Al, Cu, Ag, Au, W and of no-coating during the time t_s as a function of the accelerating voltage V. (x= 50 Å)

In the above, $y_E=x_E/R$ in I-(28) is used. Figure 8 shows the temperature-rise θ_s of a carbon specimen of volume $\pi a^2 x$ in the case of the accelerating voltage V. And also θ_s, of a carbon specimen for the case of coating with several materials (Al, Cu, Ag, Au and W) is shown in figure 9.

5. Conclusions

(1) In accordance with the elementary theory of secondary electron yield due to both incident electrons bombarding the target and the back-scattered electrons, the secondary electron emission yield can be calculated as a function of the incident energy. This information contributes to quantitatively determining the resolving power of scanning electron microscope images.

(2) Both resolving power and contrast of images in the scanning electron microscope depending on the secondary electron yield of coated films are obtained as functions of the accelerating voltage, and it is illustrated that there are minimum points in the image contrast. And the resolving power tends to decrease as the accelerating voltage increases.

(3) The energy dependence of the temperature-rise of the specimen is analytically calculated by combination of the energy loss and heat pole theories. It was found that the thermal damage increases in proportion to the incident energy in a volume under constant bombardment.

(4) The thermal damage of the specimen depends on the thermal conductivity of the specimen rather than that of the coating films assuming the same SEM operating conditions. The temperature-rise of the volume of specimen bombarded by the electron beam becomes much higher than the temperature-rise of the coating film because the beam penetrates into the specimen through the film and diffuses isotropically from the point of maximum energy loss.

(5) To obtain better resolution and to reduce temperature-rise of the specimen, ion beam sputter coating films with high secondary electron emission yields Re, Ta and W should be used. The operating conditions should be selected by estimating the temperature-rise. Subsequently, for each specimen, the operating limitation such as beam current, magnification, single frame recording time ..... all of which increase the temperature-rise of the specimen ..... and the thickness of the coating film can be determined by using equation (32).

SYMBOL TABLE

δ : secondary electron yield
δ_p and δ_B : secondary yields due to primary electrons and back-scattered electrons, respectively
δ_m : maximum yield
δ_t and δ_s : transmitted secondary electron yield and the secondary yield from the surface of a target for thin specimen
$x_D(y_D=x_D/R)$: diffusion depth
$x_C(y_C=x_C/R)$: the most probable energy dissipation depth
$x_E(y_E=x_E/R)$: maximum energy dissipation depth
$r_B(y_B=r_B/R)$: backscattering range
R : penetration range of incident electron beam
η_T, η_B and η_A : fractions of electrons transmitted, back-scattered and absorbed, respectively
Λ : mean free path for loss of a quantum of energy $\hbar\omega_p$
V(r) : potential function
Z : atomic number
n : the degree of screening (n goes from 1 to ∞)
E(or E_o) : incident energy
E_A : absorbed energy
E_B : back-scattering energy
σ : total scattering cross-section
σ_e : elastic cross-section
σ_i : total scattering cross-section due to the loss of secondary electrons
σ_p : scattering cross-section due to plasmon loss
T : energy transfer with the maximum value T_m
λ : wave length of electrons
N : the number of atoms per unit volume in the target
ρ : atomic density
A(or A_o) : atomic weight
I : ionisation energy
E_I : suitably averaged ionisation energy
E_B : mean energy of back-scattering electrons
γ : a parameter involving the effects of diffusion loss due to multiple collisions for reflected electrons and energy retardation due to electronic collisions
ν : angle of incident electron probe relative to the normal
ω_p : frequency of plasma oscillations
β : cathode brightness
C_s : spherical aberration coefficient
i_s : secondary emission current
i_o(or i_p) : primary beam current
B : brightness of a picture element on the cathode-ray tube
$\Delta B/B$: contrast between two picture elements
S_N : signal-to-noise ratio
p^2 : the total number of picture elements
T_F : total recording time per one frame
ℓ : travelling distance of secondary electrons to reach the surface
α : absorption coefficient of secondary electrons generated within the solid target

θ : angle of the direction of emerging secondary electrons; $\tan\theta=r/z$
z : distance from the surface of a target
r : distance from the center of a probe
x_α : escape depth
tem : absolute temperature of the cathode
J_c : emission current density on the cathode
θ_{ta} : temperature-rise
θ_0 : initial temperature of the specimen
κ : thermal condition coefficient
N_a : Avogadro number
$a=0.77a_H Z^{-1/6}$: screened atomic radius
a_H : the first Bohr radius of hydrogen
B_z : Boltzmann constant
E_R : Rydberg energy
Γ : Gamma function

REFERENCES

[1] Archard,G.P. (1961) Back scattering of electrons. J.Appl.Phys., 32, 1505-9.

[2] Ardenne,M.von (1959) *Tabellen der Elektronenphysik, Ionenphysik und Übermikroskopie*, Springer-Verlag, Berlin. Nos.1 and 2.

[3] Ardenne,M.Von (1962) *Tabellen zur Angewandten Physik*, Springer-Verlag, Berlin, Bd.I, 97-104.

[4] Austin,L. and Starke,H. (1902) Über die Reflexion der Kathodenstrahlen und eine damit verbundence neue Erscheinung sekundärer Emission, Ann. Phys., 9, 271-292.

[5] Baroody,E.M. (1950) A theory of secondary electron emission from metals, Phys. Rev., 78, 780-787.

[6] ———— (1955) Energy loss of medium-fast electrons in metals, Phys. Rev. Letters, 89, 910 .

[7] ———— (1956) Excitations in metals by primary electrons, Phys. Rev., 101, 1979-1984.

[8] Berger,M.J. and Seltzer,S.M. (1964) *Tables of Energy Losses and Ranges of Electrons and Positrons*, NASA, SP-3012.

[9] Bethe,H.A. (1933) *Quanten mechanik der Ein- und Zwei-Elektronen-probleme*, Handb. Phys. Springer-Verlag, Berlin, 24/2, 468-519.

[10] Bishop,H.E. (1965) A Monte Carlo calculation on the scattering of electrons in copper, Proc. Phys. Soc., 85, 855-866.

[11] Bishop,H.E. (1966) Some electron backscattering for solid target. In *X-ray Optics and Microanalysis*, Castaing, Deschamps and Philibert(Editors), Hermann, Paris, pp153-167.

[12] Bishop,H.E. (1967) Electron scattering in thick targets, Br. J. Appl. Phys., 18, 705-715.

[13] Blackstock,A.W., Ritchie,R.H. and Birkhoff, R.D. (1955) Mean free path for discrete electron energy losses in metallic foils, Phys. Rev., 100, 1078-1083.

[14] Brand,J.O. (1936) Über die Energieverteilung rückdiffundierter Kathodenstrahlen, Ann. Phys., Lpz. 26, 609-624.

[15] Brewer,G.R. (1971) The application of electron/ion beam technology to microelectronics. Some electron back-scattering for solids targets, In:IEEE Spectrum, 1, 23-37.

[16] Broers,A.N. (1970) Factors affecting resolution in the SEM, Scanning Electron Microsc. 1970; 1-8.

[17] Bronshtein,I.M. and Fraiman,B.S. (1969) *Secondary Electron Emission*, Nauka, Moscow.

[18] Bronshtein,I.M., Brozdnichenko,A.N. and Klimin,A.N. (1968) Secondary electron emission of beryllium oxide, Radio Eng. Elect. Phys.,USSR, 13, 1282-1286.

[19] Bruining,H. (1942) *Die Sekundär-Elektronen-Emission fester Körper*, Springer-Verlag, Berlin.

[20] Bruining,H. (1954) *Physics and Application of Secondary Emission*, Pergamon Press, London.

[21] Bruining,H. and De Boer,J.H. (1938) Secondary electron emission, Part I. Secondary electron emission of metals, Physica, 5, 17-30.

[22] ———— (1939a) ibid. PartVI, Compounds with a high capacity for secondary electron emission, Physica, 6, 823-33.

[23] ———— (1939b) ibid. PartV, The mechanism of secondary electron emission, Physica, 6, 834-9.

[24] Cosslett,V.E. and Thomas,R.N. (1964a) Multiple scattering of 5-30keV electrons in evaporated films, I Total transmission and angular distribution, Br. J. Appl. Phys., 15, 883-907.

[25] ———— (1964b) ibid. II Range-energy relations, Br. J. Appl. Phys., 15, 1283-300.

[26] ———— (1965) ibid. III Back-scattering and absorption, Br. J. Appl. Phys.,16, 779-96.

[27] Darlington, E.H. (1975) Backscattering of 10-100 keV electrons from thick targets, J. Phys. D: Appl. Phys., 8, 85-93.

[28] Dawson, P.H. (1966) Secondary electron yields of some ceramics, J. Appl. Phys., 37, 3644-5.

[29] Dekker, A.J. (1958) *Secondary Electron Emission*, Solid State Phys. Academic Press, New York, 6, 251-311.

[30] Dekker, A.J. and van der Ziel, A. (1952) Theory of the production of secondary electrons in solids, Phys. Rev., 86, 755-60.

[31] Dieke, G.H. (1963) *American Inst. Phys. Handb.* McGraw-Hill, New York, 7, 14-15..

[32] Dionne, G.F. (1973) Effects of secondary electron scattering on secondary emission yield curves, J. Appl. Phys., 44, 5361-4.

[33] ———— (1975) Origin of secondary-electron-emission yield-curve parameters, J. Appl. Phys., 46, 3347-51.

[34] Drescher, H. Reimer, L. and Seidel, H. (1970) Rückstreukoeffizient und Sekundärelektronen-Ausbeute von 10-100 keV-Elektronen und Beziehungen zur Raster-Elektronen mikroskopie, Z. angew. Phys. 29, 331-6.

[35] Dupouy,G. Perrier,P. Verdier,F. and Arnal,F. (1964) Transmission d'électrons monocinétiques a travers des feuilles métalliques minces, C.R.Acad. Sci. Paris, 258, 3655-60.

[36] ———— (1965) Transmission d' électrons monocinétiques a travers des feuilles metalliques minces, C.R. Acad.Sci. Paris, 260, 6055-60.

[37] Ebert,P.J. Lauzon,A.F. and Lent,E.M. (1969) Transmission and backscattering of 4.0-to 12.0-MeV electrons, Phys.Rev., 183, 422-30.

[38] Ehrenberg,W. and Franks,J. (1953) The penetration of electrons into luminescent material, Proc.Phys.Soc. B 66, 1057-66.

[39] Ehrenberg,W. and King,D.E.N. (1963) The penetration of electrons into luminescent materials, Proc.Phys. Soc. B 81, 751-66.

[40] Everhart,T.E. (1960) Simple theory concerning the reflection of electrons from solids, J.Appl.Phys. 31, 1483-90.

[41] Everhart,T.E. and Hoff,P.H. (1971) Determination of kilovolt electron energy dissipation *vs* penetration distance in solid materials, J. Appl.Phys. 42, 5837-46.

[42] Everhart,T.E. Wells,O.C. and Oatly,C.W. (1959) Factors affecting contrast and resolution in the scanning electron microscope, J.Electronics and Control, 7, 97-111.

[43] Everhart,T.E. and Hayes,T.L. (1972) The scanning electron microscope, Sci.Amer., 226, 54-69.

[44] Ferrell,R.A. (1956) Angular dependence of the characteristic energy loss of electrons passing through metal films, Phys.Rev., 101, 554-63.

[45] Fitting,H.-J. (1974) Transmission, energy distribution, and SE excitation of fast electrons in thin solid films, Phys.Stat.Solidi(a) 26, 525-35.

[46] Frederikse,H.P.R. (1965) *American Inst. Phys. Handb.* McGraw-Hill, New York, §9 pp.158-9.

[47] Fröhlich,H. (1932) Theorie der Sekundärelektronemission aus Metallen, Ann.Physik, 13, 229-48.

[48] Ganachaud,J.P. (1977) These d'Etat, Universite de Nantes.

[49] Ganachaud,J.P. and Caillier,M. (1975a) 2e Colloq.Int.Phys.Cimie des Surfaces, Brest

[50] ——————— (1975b) Le Vide 30A3

[51] Glendenin,L.E. (1948) Determination of the energy of beta particle and photons by absorption, Nucleonics, 2, 12-32.

[52] Gobrecht,H. and Speer,F. (1953) Ein Beitrag zur Sekundärelektronenemission von Störstellenhalbleitern, Zeit.Phys. 135, 602-614.

[53] Hachenberg,O. and Brauer,W. (1959) *Secondary Electron Emission from Solids*, Adv. Electronics & Electron Phys. 11, 413-99.

[54] Hohn,F.J. and Niedrig,H. (1972) Film thickness determination of small areas by electron backscattering, Proc.5th Europ.Congr. on Elec. Micr., Inst. Physics, Bristol, U.K., 358-9.

[55] Holliday,J.E. and Sternglass,E.J. (1959) New method for range measurements of low-energy electrons in solids, J.Appl.Phys., 30, 1428-31

[56] Jahrreiss,H. (1964) Über einige Erweiterungsmöglichkeiten der Sternglassschen Theorie der Sekundärelektronenemission und deren empirische Prüfbarkeit, Ann. Phys., 14, 325-52.

[57] Jonker,J.L.H. (1952) On the theory of secondary electron emission, Philips Res.Rep., 7, 1-20.

[58] ——————— (1954a) The similarity law of secondary emission, Philips Res.Rep., 9,391-402.

[59] ——————— (1954b) The angular distribution of the secondary electrons of soot, Philips.Res.Rep. 9, 434-40.

[60] Johnson,J.B. and McKay,K.G. (1954) Secondary electron emission from germanium, Phys. Rev. 93, 668-72.

[61] Kanaya,K. and Okayama,S. (1972) Penetration and energy-loss theory of electrons in solid targets, J.Phys.D: Appl.Phys., 5, 43-58.

[62] Kanaya,K. and Kawakatsu,H. (1972) Secondary electron emission due to primary and backscattered electrons, J.Phys.D:Appl.Phys., 5, 1727-42.

[63] Kanaya,K. and Ono,S. (1974) Secondary electron emission from solid surfaces by bombardment with charged particles, J.J.Appl.Phys. 5, 944-49.

[64] ——————— (1976) Consistent theory of electron scattering with atoms in electron microscopes, J.Phys.D:Appl.Phys.,9 , 161-74.

[65] ——————— (1978) The energy dependence of a diffusion model for an electron probe into solid targets, J.Phys.D:Appl.Phys. 11, 1495-508.

[66] Kanaya,K. Ono,S. and Ishigaki,F. (1978) Secondary electron emission from insulators, J. Phys.D:Appl.Phys., 11, 2425-37.

[67] Kanter,H. (1957) The backscattering of electrons in the energy range from 10 keV to 20 keV, Ann.Phys., 20, 144-66.

[68] ——————— (1961a) Energy dissipation and secondary emission in solids, Phys. Rev. 121, 677-80.

[69] ——————— (1961b) Contribution of backscattered electrons to secondary electron formation, Phys.Rev., 121, 681-4.

[70] Katz,L. and Penfold,A.S. (1952) Range-energy relations for electrons and the determination of beta-ray and end-point energies by absorption, Rev.Mod.Phys., 24, 28-44.

[71] Klein,C.A. (1968) Backscattering of kilovolt-electron beams, Raytheon Co. Tech.Mems. Raytheon Co.T-786, 1-8.

[72] Knoll,M. (1935) Aufladepotential und Sekundäremission elektronenbestrahlter Körper, Z.Tech.Phys. 16, 467-75.

[73] Knoll,M. Hachenberg,O. and Randmer,J. (1944) Mechanism of secondary emission in the interior of ionic crystals, Z.Phys., 122, 137-162.

[74] Kollath,R. (1956) *Secondary Electron Emission of Solids Induced by Electron Bombardment*, Encyclopedia of Phys. Springer-Verlag, Berlin, 21, 232-303.

[75] Koshikawa,T. and Shimizu,R. (1973) Secondary electron and backscattering measurements for polycrystalline copper with a spherical retarding-field analyser, J.Phys. D: Appl. Phys., 6, 1369-80.

[76] Kulenkampff,H. and Rüttiger,K. (1954) Enegie-und Winkelverteilung rückdiffundierter Elektronen, Z.Phys., 137, 426-34.

[77] Kulenkampff,H. and Spyra,W. (1954) Energieverteilung rückdiffundierter Elektronen, Z.Phys., 137, 416-25.

[78] Lane,R.O. and Zaffarano,D.I. (1954) Transmission of 0-40 keV electrons by thin films with application to beta-ray spectroscopy, Phys. Rev., 94, 960-4.

[79] Lenard,P. (1918) *Quantitatives über Kathodenstrahlen aller Geschwindigkeiten*, Karl Winters Univ. Buchh. Heidelberg.

[80] Lenard,P. (1895) Über die Absorption der Kathodenstrahlen, Z. für Phys.,56, 255-75.

[81] Lenz,F. (1954) Zur Streung mittelschneller Elektronen in kleinste Winkel, Z.Naturforg., 9a, 185-204.

[82] Llacer,J. (1968) *SLAC Rept. No.86*, Stanford: Linear Accelerator Centre.

[83] Lonergan,J.A. Jupiter,C.P. and Merkel,G. (1970) Electron energy straggling measurement for thick targets of Be,Al and Au at 4.0 and 8 MeV, J.Appl.Phys., 41, 678-688.

[84] Lye,R.G. and Dekker,A.J. (1957) Theory of secondary emission, Phys.Rev., 107, 977-81.

[85] Marshall,J.F. (1952) The theory of secondary emission ,Phys. Rev., 88, 416-7.

[86] Marton,L. Leder,L.B. and Mendlowitz,H. (1954) *Characteristic Energy Losses of Electrons in Solids*, Adv.Electronics & Electron Phys. Academic Press, New York, 6, 183-238.

[87] McKay,K.G. (1948) *Secondary Electron Emission*, Adv. Electronics, 1, 65-130.

[88] Meister,H. (1958) Zur Theorie Absorption monoenergetischer Elektronen in metallischen Folien, Z.Naturforg. 13a, 809-20.

[89] Nakhotkin,N.G. Ostroukhov,A.A. and Romanovsky,V.A. (1962) Fizika Tverdogo Tela 4, 1514-23.

[90] ———— (1963) ibid, 5, 41-47.

[91] ———— (1965) ibid, 7, 210-216.

[92] Niedrig,H. and Sieber,P. (1971) Rückstreuung mittelschneller Elektronen an dünnen Schichten, Z.angew.Phys. 31, 27-37.

[93] Oatley,C.W. and Pease,R.F.W. (1965) *Scanning Electron Microscopy*, Adv. Electronics & Electron Phys. Academic Press, New York, 21, 181-247.

[94] Ono,S. Arakawa,S. Harada,Y. Adachi,K. and Kanaya,K. (1974a) Image resolution and thermal damage of coated films in scanning electron microscope, 8th Inter. Con. on Elec. Micr.Canberra, 2, Australian Academy of Science, Canberra, 686-7.

[95] Ono,S. and Kanaya,K. (1974b) Image resolution and thermal damage of coated films in SEM, Research Rep. Kogakuin Uni. 37, 243-54.

[96] Ono,S. Sugawara,Y. and Kanaya,K. (1977) Further investigation on image resolution and thermal damage of coated films considering back-scattered effects in SEM, Research Rep.Kogakuin Uni. 42, 123-35.

[97] Ono,S. and Kanaya,K. (1979) The energy dependence of secondary emission based on the range-energy retardation power formula, J.Phys.D: Appl.Phys. 12, 619-31.

[98] Pease,R.F.W. and Nixon,W.C. (1965) High-resolution scanning electron microscopy, Sci.Instr. 42, 81-85.

[99] Petzel,B. (1958) Thesis Dresden

[100] Pillon,J. and Ganachaud,J.P. (1977) Secondary electron emission of metal surface (Al, Ag, Au), Proc. 7th Int. Vac. Congr. I, 7th Int. Vac. Congr. Comm., Vienna, 473-76.

[101] Pines,D. and Bohm,D. (1952) A collective description of electron interactions II Collective *vs* indivisual particle aspects of interactions Phys. Rev. 85, 338-53.

[102] Radzimski,Z. (1978) The backscattering of 10∿120 keV electrons for various angles of incidence, Acta Physica Polonica, 6, 783-90.

[103] Rauth,A.M. and Simpson,J.A. (1964) The energy loss of electrons in solids, Radiation Res. 22, 643-61.

[104] Reimer,L. (1968) Monte-Carlo-Rechnungen zur Elektronen Diffusion, Optik, 27, 86-98.

[105] Rester,D.H. and Derrickson,J.H. (1971) Electron transmission measurement for Al,Sn and Au targets at electron bombarding energies of 1.0 and 2.5 MeV. J.Appl. Phys. 714-721.

[106] Ritchie,R.H. (1973) Plasmon losses by fast electrons in thin films, Phys.Rev. 106,874-80.

[107] Rose,A (1948) *Television Pickup Tubes and the Problem of Vision*. Adv. in Electronics, Vol I, Academic Press New York, 131-165.

[108] Salow,H. (1940) Angular dependence of the secondary electron emission from insulators, Z. Phys. 41, 434-42.

[109] Seiler,H. (1967) Einige aktuelle Probleme der Sekundärelektronenemission, Z. angew. Phys. 22, 249-63.

[110] Seliger,H.H. (1955) Transmission of positrons and electrons, Phys.Rev. 100, 1029-37.

[111] Shimizu,R. (1974) Secondary electron yield with primary electron beam of kilo-electron-volts, J.Appl.Phys. 45, 2107-11.

[112] Shimizu,R. and Murata,K. (1971) Monte Carlo calculations of the electron-sample interactions in the scanning electron microscope, J.Appl.Phys. 42, 387-94.

[113] Shockley,W. and Pierce,J.R. (1938) A theory of noise for electron multipliers, Proc. IEEE 26, 321-32.

[114] Simon,R. (1969) Resolving power of the scanning electron microscope, J.Appl.Phys. 40, 2851-56.

[115] *Smithsonian Physical Tables* (1954) 9th ed.

[116] Spencer,L.V. and Fano,V. (1954) Energy spectrum resulting from electron slowing down, Phys.Rev. 93, 1172-81.

[117] Spencer,L.V. (1955) Theory of electron penetration, Phys. Rev. 98, 1597-1615.

[118] Spencer,L.V. (1959) Energy dissipation by fast electrons NBS Monograph No.1.

[119] Sternglass,E.J. (1950) Secondary electron emission and atomic shell structure, Phys.Rev. Letter. 80, 925-6.

[120] ———— (1954) Backscattering of kilovolt electrons from solids, Phys.Rev. 95, 345-58.

[121] ———— (1957) Theory of secondary electron emission by high speed ions, Phys.Rev. 108, 1-12.

[122] Thomas, S and Pattinson,E.B. (1970) Range of electrons and contribution of back-scattered electrons in secondary production in aluminium, J,Phys D: Appl.Phys. 3, 349-57.

[123] Tomlin,S.G. (1963) The back-scattering of electrons from solids, Proc.Phys.Soc.Letter, 82, 465-66.

[124] Verdier,P. and Arnal,F. (1968) Phénomene de retrodiffusion délectrons mono cinétiques, C.R.Acad.Sci.Paris, 267, 1443-6.

[125] ———— (1969) Physique corpusculaire-calcul du coefficient de rétrodiffusion dans le cas d'électrons mono cinétiques CR.Acad.Sci.Paris, 268 1101-4.

[126] Vyatskin,A.Ya. and Trunev,V.V. (1967) Radioteknika i Elektronika,12, 1636-41.

[127] ——————————— (1970) Radioteknika i Elektronika, 15, 565-70.
[128] ——————————— (1972) Radioteknika i Elektronica, 17, 1899-1905
[129] Weinryb,E. and Philibert,J. (1964) Mesure du coefficient de rétrodiffusion des électrons de à 30 keV. C.R.Acad.Sci.Paris 258, 4535-8.
[130] Wells,O.C. et al. (1974) *Scanning Electron Microscopy*, McGraw-Hill, New-York, 69-107.
[131] Wittry,D.B. (1966) Secondary electron emission in the electron probe, *X-ray Optics and Microanalysis*, (Castaing,R.Deschamps,P. and Philibert,J.Edtors) Hermann, Paris, p.168.
[132] Wittry,D.B. (1970) Electron beam interactions in solids, Scanning Electron Microsc.1970; 409-415.
[133] Wittry,D.B. and Kyser,D.F. (1967) Measurement of diffusion lengths in direct-gap semiconductors by electron-beam excitation, J.Appl.Phys. 38, 375-82.
[134] Wolff,P.A. (1954) Theory of secondary electron cascade in metals, Phys.Rev. 95, 56-66.
[135] Wooldridge,D.E. (1939) Theory of secondary emission, Phys.Rev. 95, 562-78.
[136] Wright,K.A. and Trump,J.G. (1962) Backscattering of megavolt electrons from thick targets, J.Appl.Phys. 33, 687-90.
[137] Young,J.R. (1956a) Penetration of electrons and ions in aluminium, J.Appl.Phys. 27, 1-4.
[138] ——————— (1956b) Dissipation of energy by 2.5-10 keV electrons in Al_2O_3, J.Appl.Phys. 27, 524-25.
[139] ——————— (1956c) Penetration of electrons in aluminium oxide films Phys.Rev. 103, 292-93.
[140] Zeitler,E. and Bahr,G.F. (1959) Contributions to quantitative electron microscopy, J.Appl. Phys. 30, 940-44.
[141] van der Ziel,A. (1953) A modified theory of production of secondary electrons in solids, Phys.Rev. 92, 35-9.

Discussions with reviewers

Radzimski,Z.: (1) How are both the depth of maximum energy dissipation y_E and the depth of most probable energy dissipation y_C used to estimate the diffusion sphere centre?
Authors: It is derived so that the diffusion sphere centre agrees with the experimental results.

Radzimski,Z.: (2) How was the eq.(23) (in chapter I) for the back-scattering range r_B obtained?
Authors: It is determined on the basis of an empirical analysis.

Radzimski,Z.: (3) Only the values of y_D y_E and r according to the description under Fig.13 were calculated from eq.(20),(22) and (17) respectively. The values of y_C and y_B are the parameters of the diffusion model and they don't follow from the theory presented.
Authors: Yes, we agree with your comment. The values of y_C and y_B don't follow from the analytical calculations. They are determined according to the geometrical relationship of diffusion model.

Radzimski,Z.: (4) Does the assumption y=1/2 in calculation of the backscattering coefficient $r=\eta(y=1/2)$ from equation (17) have any physical meaning ?
Authors: It is defined that a half of the range y=x/R=1/2 means the limit where incident electrons are backscattered.

Wittry,D.B.: (1) For the data used, the model proposed seems to work as well as some other models based on diffusion, and better than most of the diffusion models. However some of the most critical tests have not been applied to the present model such as a comparison with the experimental results for X-ray production with depth and the energy distribution of backscattered electrons. Many of the assumptions used are not explained or justified. The assumption that plasmon losses can be neglected is not justified for light elements. Moreover, the average excitation energy certainly covers a much wider range than 100-200eV quoted in the paper.
Authors: In the model for electron penetration into solid targets, the energy loss involves the plasmon loss as well as ionization loss. In general, the peaks of plasmon loss is very high, but the ionization loss dominates the total amount of losses. Then, the experimental data shown in the paper by Kanaya and Ono(1976) (see Fig.8 in this reference) is used for the analysis. The plasmon loss is about 10% of the ionization loss for the range of incident energy greater than about 100eV.

Wittry,D.B.: (2) It is unreasonable to expect the same diffusion model to apply for energies of 100eV to 10MeV and atomic number Z from 4 to 80 (re. Fig.14). The authors have failed to recognize that any diffusion model has a limited range of application.
Authors: The energy retardation power formula represents the whole energy range. Especially, for the parameter n=1 it exactly agrees with the Bethe retardation formula. The diffusion model is considered to be a reasonable model in the high energy range, though the theoretical and experimental comparison is not satisfactory.

Wittry,D.B.: (3) It does not appear that the diffusion model used by the authors will be widely accepted because they chose to ignore the Bethe retardation law and to derive a new expression for dE/dx. They have also neglected plasmon losses which are obviously important at low Z and also make a significant contribution at higher Z. (the plasmon losses are included when the Bethe retardation law is used - if the mean excitation energy is experimentally determined).
Authors: The plasmon losses are dominant at low energy range for low atomic number materials. For such cases, both plasmon and ionization losses should be taken into account according to the comment.